Development of a Centrifugal Microfluidic System for Rapid On-Site Analysis of Environmentally Important Species

Angela LaCroix-Fralish

A Thesis
in
The Department
of
Chemistry and Biochemistry

Presented in Partial Fulfillment of the Requirements
for the Degree of Master of Science (Chemistry) at
Concordia University
Montreal, Quebec, Canada

January 2009

Your file Votre référence
ISBN: 978-0-494-63318-2
Our file Notre référence
ISBN: 978-0-494-63318-2

ABSTRACT

Development of a Centrifugal Microfluidic System for Rapid On-Site Analysis of Environmentally Important Species

Angela LaCroix-Fralish

Micro-total analysis systems (μTAS) have enabled the miniaturization and simplification of environmental contaminant detection methods. Reduced reagent and sample consumption, speed of analysis, and field portability are only a few of the advantages μTAS systems provide. Centrifugal microfluidics have the added advantages of using centrifugal force for moving liquids, thereby avoiding solvent and filtration problems encountered with the electroosmotic flow typically used in μTAS manifolds. These properties suggest that centrifugal μTAS systems may offer many advantages as analysis platforms for the on-site analyses of a variety of important environmental pollutants.

A model instrument has been developed and characterized for rapid, classical spectrochemical reactions. The system is designed for the determination of nitrite, nitrate and hexavalent chromium, three common pollutants. The system uses a single disc that requires 100μl of sample per analyte using a centrifugal disc that filters the water sample which is then mixed with the appropriate reagents in one or two steps using capillary valves, and is detected on-disc with a pathlength of 1.04 mm. Using a multi-wavelength technique for the precise determination of the reference signal, the detection limits for these three systems are 0.008, 0.6, and 0.03 $mg \cdot L^{-1}$ for NO_2^--N, NO_3^--N, and Cr^{6+} respectively. A comparison between this technique and several conventional techniques highlights the strengths and limitations of the system.

ACKNOWLEDGEMENTS

To the members of the Salin and Skinner labs for sharing your knowledge and your friendship with me. None of this research would have been possible without your assistance, support and encouragement.

To my supervisors and mentors Dr. Eric Salin and Dr. Cameron Skinner, you both took a chance on the biologist who wanted to be a chemist. Thank you for your encouragement, advice and your endless hours of answering questions.

To my committee members, Dr. Yves Gélinas and David Burns. Your comments and ideas have helped to shape this research. Thank you for taking the time to thoughtfully consider all the facets of this research.

To Josiane, for helping me with some of the concepts I just couldn't get on my own and encouraging me to have more self confidence.

To Maria, for your support, knowledge and friendship. Your humor and encouragement will always be appreciated.

To my family who always encouraged me to pursue my interests even if they were not theirs. Your prayers, conversations, and visits were appreciated.

To my friends and Montreal family, especially, the Belley's, the Lessard's and the Mellette's. For feeding me on numerous occasions and helping me realize that life is more than just goals, thank you for your support, your cooking skills, and your friendship.

And lastly, to my husband, Dr. Michael LaCroix-Fralish. Who brought me dinner and kept me company during study sessions. You are the best husband a master's student could ask for.

TABLE OF CONTENTS

LIST OF FIGURES

LIST OF TABLES

LIST OF EQUATIONS

ABBREVIATIONS

A – Absorbance
AU – Absorbance units
CCD – Charge Coupled Device
CD – Compact Disc
CNC – Computer Numerical Control
DL – Detection Limit
DVD – Digital Video Disc
DXF – Drawing Exchange Format
ECD – Electrochemical Detection
EOF – Electrosmotic Flow
EPA – Environmental Protection Agency
FT – Fourier Transformation
FIA – Flow Injection Analysis
I – Intensity
IR – Infrared
NO_2^--N – Nitrite calculated as Nitrogen
NO_3^--N – Nitrate calculated as Nitrogen
PDA – Photodiode Array
PDMS – Poly(dimethylsiloxane)
RPM – Revolutions Per Minute
RSD – Relative Standard Deviation
S/N – Signal-to-Noise Ratio
SMA – SubMiniature version A connector
T – Transmittance
TIT – Total Integration Time
UV – Ultraviolet
VIS – Visible
μFIA – Micro-Flow Injection Analysis
μTAS – Micro-Total Analysis Systems

Chapter 1

INTRODUCTION AND OBJECTIVES

1.1 The Nitrogen Cycle

Pollution of commercial, municipal and recreational waterways has long been a recognized problem. Reactive nitrogen (N) species have been studied for many years as a large source of air, land and water pollution. They affect everything from environmental considerations to food production and disease control. For this reason, the control of nitrogen sources is a major public policy challenge.[1]

The Nitrogen Cycle is thought to be the most complex cycle of all the major elements [2] as nitrogen has seven oxidation states, numerous mechanisms for interspecies conversion, and a variety of transport and storage processes. Recent studies have shown that human activities increasingly dominate the environmental nitrogen budget at global, regional and local scales.[3] The greatest impacts are directly from fertilizers used to increase food production. Indirect sources are predominantly through the combustion of fossil fuels, which emit NO as a waste product. Both of these processes have increased by more than a factor of 10 since the beginning of the 19^{th} century. The most abundant (78%) form of nitrogen is gaseous diatomic nitrogen (N_2) and is not bioavailable due to the strong triple bond.[3] Therefore, the most common human alteration to the nitrogen cycle is through the addition of bioavailable nitrogen in the form of ammonia (NH_3). It is applied as a fertilizer which goes through the process of nitrification and can be converted to nitrite (NO_2^-) which subsequently gets oxidized to nitrate (NO_3^-). Nitrogen may also follow a denitrification cycle from NO to N_2O to N_2, which can eventually lead

back to NH_3 or be sunk into one of many environmental reservoirs.[4] These processes are controlled by chemical conditions, biological nitrogen fixation, and fixation of atmospheric N_2 by lightning. Because the nitrogen budget is not in steady state equilibrium [5], and because it has such a large anthropogenic and environmental impact, it is of utmost importance to increase our understanding of the amounts and species of nitrogen species found in the environment.

1.2 Nitrate and Nitrite Species

The detection of nitrate and nitrite plays a significant role in the overall study of reactive nitrogen species. Both species are highly soluble and inexorably linked to each other. In fact, it is rare that one is found without the other.[6] Detection of nitrate and nitrite in water and wastewater is of particular importance for environmental protection, commercial ventures, and biomedical applications.

In the environment, the detection of NO_3^- is important to limnologists because it is the major form of reactive nitrogen in waters and is a major nutrient for primary productivity.[7] Contamination of natural waters from anthropogenic sources of nitrogen is an extensive problem. The excess nutrients can cause eutrophication of lakes and estuaries leading to an imbalance in the natural food and life cycles of organisms. Algal blooms can result in high levels of cyanobacteria and other toxic microorganisms leading to dead zones, unusable recreational waterways, and commercial fish kills. Nitrate and nitrite are often found in industrial effluent as a byproduct of a number of applications. Common industrial uses of nitrate and nitrite include: corrosion inhibitors in boiler systems, as a curing agent for meat, and in the production of explosives.[6,8-10]

Consumption of nitrate and nitrite in contaminated drinking water can lead to a range of health effects. It can cause the oxidation of iron in hemoglobin producing methemoglobinemia, also known as "blue baby syndrome", when an infant can die from asphyxia.[12] Nitrite activity with secondary and tertiary amines already present in the body can form N-nitrosamines, which are potential carcinogens.[13] In biomedical applications, nitrate is also used as a stable end product in many physiological studies.[11]

For all of these reasons, the World Health Organization has imposed a limit of 10 $mg{\cdot}L^{-1}$ nitrate (as nitrogen) and 1 $mg{\cdot}L^{-1}$ nitrite (as nitrogen). However, many fresh and waste waters throughout the world now exceed this and even stricter national or regional regulatory limits exist.[14] Consequently, there is a great need to monitor these nitrogen species in both the laboratory and directly in the field.

1.3 Detection of Nitrate and Nitrite

Because nitrite and nitrate have such a large impact on environmental, social and economic issues, they have been widely studied and their detection is well characterized in the literature. There is a large number of current methods described for the detection of nitrite and nitrate; individually, sequentially or simultaneously. Because these nitrogen species are so ubiquitous, the majority of literature methods are for matrix-dependent or method specific samples.[6] A brief introduction is given here to provide an overview of the detection strategies that are currently used. The standard method for reporting aquatic nitrogen loading uses the amount nitrate or nitrite calculated as N (nitrogen). For example, 1 $mg{\cdot}L^{-1}$ NO_2^- would be reported as 0.3 mg L^{-1} NO_2^--N or the amount of nitrogen in the sample as nitrite. This is used to avoid any quantitative inconsistencies

due to the molar mass difference in the two species. The standard convention is followed in this thesis.

1.3.1 Detection of Nitrite

NO_2^- usually exists in oxic H_2O at low concentrations and is mainly detected to help calculate the flux of nitrification and denitrification processes or as an intermediate in the oxidation or reduction of NO_3^- and NH_4^+.[15] Moorcroft *et al.*[6] reported 35 different methods for the detection of nitrite alone. These methods include the derivatization of nitrite for visible detection, reduction of nitrite to NO for chemiluminescence detection,[16] as well as fluorescence reactions and electrochemical detection (ECD) (Figure 1.1).

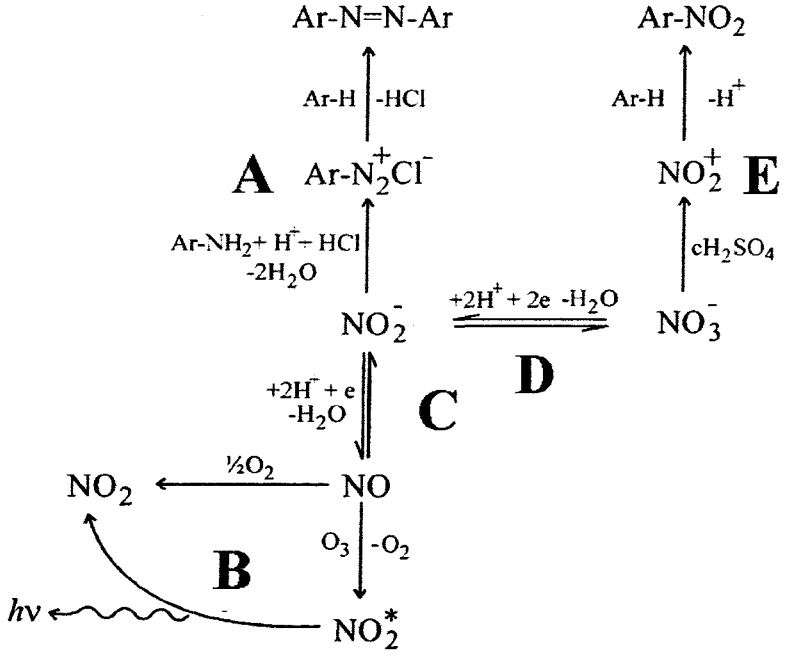

Figure 1.1 Common pathways for the detection of nitrite and nitrate. (***A***) Griess reaction, (***B***) chemiluminescence, (***C***) denitrification to NO, (***D***) reduction of NO_3-, (***E***) alternate derivatization strategy. Adapted from Moorecroft *et al.*, 2001.

The majority of environmental methods use some form of the Griess reaction for derivatization of nitrite. The original reaction consists of the diazotizing of sulfanilic acid by nitrite followed by azo coupling with 1-naphthylamine in an acidic solution.[17,18] This method has been constantly modified and improved since its inception in the late 1800's.[11,19] Uses of carcinogenic reagents and large amounts of waste reagents in this reaction have recently seen the call for "greener" procedures. These procedures include the oxidation of iodide in solution with nitrite[12] and novel electrophonic coupling reagents.[13] However, the standard method for nitrite detection remains the colorimetric Griess reaction, with detection by ion chromatography as a secondary option. [20]

1.3.2 Detection of Nitrate

The methods for direct determination of nitrate are diverse and are generally suited for a very specific matrix or have relatively complex procedures. They include: capillary electrophoresis,[21] gas chromatography, ultra-violet spectroscopy (UV),[22,23] visible spectroscopy (VIS),[24] infrared spectroscopy (IR) and Raman spectroscopy, as well as electrochemical detection.[25] Of all of these methods, electrochemical detection is the most common direct detection strategy for nitrate.[6] Detection by UV spectroscopy, a nitrate-selective electrode, or reduction by cadmium or hydrazine remain the only approved standard methods.[20]

Due to the relatively stable nature of NO_3^-, indirect detection by reduction to NO_2^- followed by some form of the Griess reaction is by far the most common detection strategy (Figure 1.1). The reduction procedure is known to be complicated and multiple papers have been written on the techniques used in both chemistry and industrial applications.[26] Photochemically-induced reduction of nitrate is the most environmentally

friendly strategy, but only has reduction efficiencies of about 70-84%.[27] Enzymatic and bacterial reduction have also been reported, but require specialized laboratories for cell growth.[28,29] Multiple metals have been employed in redox reactions with the highest number of papers using cadmium.[30-35] Although cadmium remains the standard, it is known to be toxic to organisms. Thus, zinc is often utilized as an alternative reducing agent.[8,15,36-38]

The detection of nitrate and nitrite has received considerable attention as they are such important species to the well being of humans and the environment. The most common protocol for their determination remains the detection of nitrite with a modified Greiss reaction followed by bulk reduction of the sample to nitrite using cadmium metal and detection of nitrate from the difference. This is the method used in this research because of its simplicity and its applicability to miniaturization and automation.

1.4 Detection of Hexavalent Chromium

Nitrite and nitrate are harmful only in relatively large quantities, but multiple chemical species, such as hexavalent chromium (Cr^{6+}) are harmful in even small amounts. To validate the single step reaction process and general disc design, Cr^{6+} was investigated. Natural and drinking waters become contaminated with chromium (VI) as a result of untreated or under treated industrial effluent discharged into waterways. Consumption of contaminated waters leads to toxic and carcinogenic affects for both humans and animals.[68] For this reason the EPA and Health Canada have imposed a limit of 0.05 $mg \cdot L^{-1}$ for drinking water. Hexavalent chromium was an ideal choice based on its well known and simplistic detection strategy using diphenylcarbazide to derivatize the ion.[69,70] This detection strategy is one of two approved standard methods, the other being

ion chromatography.[20] The laboratory work on hexavalent chromium was performed by Jennifer Clare and Michal Shivit under the guidance of the author. All experimental design, data interpretation and conclusions were drawn by the author.

1.5 Microfluidics

As a relatively new field, microfluidics presents an opportunity to develop a portable and practical method for the detection of nitrite and nitrate. Such a method would help researchers understand the positive and negative consequences of nitrogen in our environment. Here a brief background on microfluidics and current microfluidic devices for nitrate and nitrite is presented, along with a more detailed description of centrifugal microfluidics which is used in this thesis.

Microfluidics is the study of sub-milliliter amounts of fluid and/or sub-millimeter sized devices where the small scale results in changes of fluid behavior. This size scale effect generally occurs when features are on the order of 10 s to 100 s of micrometers (μm). Due to scaling laws in these devices, typically important laws and forces (such as gravity) become largely unimportant while surface forces (such as capillary action) tend to dominate. Microfluidics utilizes these laws to discover new effects and increase instrument performance, while compensating for difficulties seen at the miniature scale, such as low Reynold's numbers that cause laminar flow and poor mixing. The dramatic decrease in instrument and sample size also allows faster analysis and specialized detection schemes that, in turn, allow compact, efficient, and portable systems.[39,40]

Conventionally, only the fluid components of microfluidic devices need to be miniaturized, while the rest of the instrument can be of any size.[41] When an entire analysis system is miniaturized (from pretreatment to detection), it is referred to as a

micro-total analysis system (μTAS) or "lab-on-a-chip". Descriptions of μTAS systems have been increasing dramatically since their inception in the early 1990's by Manz *et al.*[42] The majority of the work described in the literature is performed on simple planar microchips fabricated from silicon or polymers, but this has increasingly changed over recent years, depending on the application.[43] Microfluidic and μTAS systems have largely been developed for biomedical applications such as diagnostic detection of nucleic acids, proteins, cells, and tissue samples. Microfluidics has only recently seen a substantial increase in adoption in the field of environmental chemistry.[44]

Due to the increasing demand for information on environmental conditions, there is a need for real time, *in situ* analysis techniques. Microfluidics provides a reliable means of detecting environmentally important species directly in the field. The small volume, coupled with disposability and portability of the devices, increases the number of samples that can be analyzed while simultaneously decreasing or eliminating analyte loss and contamination from transportation and storage. This results in the ability to take accurate, high resolution temporal and spatial measurements.[45] Flow-injection analysis (FIA) coupled with spectrophotometry or ECD feature prominently as analysis/detection strategies for environmental μTAS systems.[46] FIA allows the continual monitoring of samples through an online flow system with little operator involvement. Understanding of the physics that applies to microfluidic systems and their capabilities has increased dramatically over the last decade providing improved analytical strategies for the analysis of diverse analytes encountered in the wide range of matrices found in environmental samples.[47] However, there is still a further need for research into developing more robust microfluidic strategies for the analysis of complex matrix samples.

1.5.1 Microfluidics for Nitrate and Nitrite Analysis

Currently there are multiple published methods for the determination of either nitrite (NO_2^-) alone or nitrate (NO_3^-) and nitrite (NO_2^-) sequentially using microfluidics or μTAS. The majority of these devices feature spectrophotometric nitrite detection, using a μFIA analysis system coupled with micro-cadmium columns or frits directly on the chip.[48-52] μECD is the second most common detection strategy for nitrite and nitrate on chip based microfluidic devices.[25,53-55] The main application for these systems is nutrient analysis in natural waters [56,57] although there are several specifically designed devices for wastewater analysis.[58] There are several published studies using nitrite as a proof-of-concept analyte for novel micro-systems. The linear dynamic range and detection limit depend on the specific application and device but are generally from 0 - 5 mg L^{-1} NO_3^--N and 0.0004 - 1 mg L^{-1} NO_2^--N, respectively. Fewer detection limits were reported for nitrate as most papers focused solely on nitrite.

The previously described systems are generally focused on the actual detection of nitrite or nitrate and few include common sample manipulation steps such as clearing of the sample via filtration or sedimentation on the chip. The majority of these studies also use large external equipment for fluid movement. A few studies described the use of multiple piezoelectric micropumps or syringes for fluid movement, but most depend on external pumps or electrosmotic flow (EOF). All required a high voltage source, multiple complex microstructures, or large external equipment for pumping capabilities.

1.5.2 Centrifugal Microfluidics

Centrifugal microfluidics use centripetal force to move liquid elements through a microfluidic disc. This eliminates the common pumping and mixing problems found in

typical chip based microfluidic systems while retaining the capabilities of valving, flow splitting, separation, droplet formation, and incubation. Centrifugal microfluidics can be used for the same types of applications as chip based microfluidics. Fluid injected onto the disc near the axis of rotation is propelled towards the outside of the disc by centrifugal force. Detailed descriptions of the equations governing the applicable pseudo-forces (Centrifugal, Euler and Coriolis) can be found in Madou *et al.* (2006) and Ducree *et al.* (2007). Much of the following theory has come from these two papers. Only a cursory overview of several of the capabilities of centrifugal microfluidics is presented here to demonstrate the reason this platform was chosen for the device developed in this thesis.

1.5.3 Sedimentation

Centrifugal force has been used for sedimentation in numerous applications, both micro- and macrofluidic. Application of centrifugal force is the principle behind the centrifuge, the workhorse of biological and physical sciences. In the analytical realm, it is generally performed off-chip for conventional microfluidic applications to avoid clogging and contamination of the microfluidic channels. Sedimentation on microfluidic discs has the caveat that sedimentation occurs in the outward direction as opposed to the downward direction. Environmental samples, especially those generally taken for the analysis of nitrite and nitrates, can contain large amounts of soils or other suspended particulate matters. Thus including sedimentation directly on the disc can eliminate at least one exterior sample preparation step leading to faster, simpler analysis of the samples.

1.5.4 Fluid Control

The ability to use centripetal force to move liquid through the device increases the number of fluid and matrix types available for analysis. Centripetal force generated flow is relatively insensitive to the pH, chemical properties, and ionic strength of the liquid unlike mechanical or EOF generated flows. This is an important advantage as these can be limiting factors in chip based fluid movement. The main considerations for movement by centrifugally induced pressure are the geometry and location of the channels/reservoirs, density of the liquid (ρ), and the rotation rate or angular velocity (ω). When the centripetal pressure (Equation 1) overcomes the ambient pressure on a fluid head, the liquid moves towards the outside of the disc. By using various combinations of speed and channel geometry various flow rates can be achieved. The volumetric flow rate and velocity of the liquid can also be calculated from theoretical equations detailed in Duffy *et al.*[59] Moving liquid by centripetal forces also eliminates any external pumps and almost all off disc handling.

$$P_m = \rho\omega^2 \bar{r}\Delta r$$

P_m = centripital pressure at miniscus
ρ = density
ω = angular velocity
$\bar{r}$ = mean radial position
Δr = length of round radial channel

Equation 1.1 Liquid pressure on liquid head induced from centripetal forces exerted on a liquid when rotated.

1.5.5 Valving and Volume Control

If channels of narrow dimensions, are made, or modified to be hydrophilic, with chemicals or materials such as glass or quartz, positive capillarity effect can be used to move microliter quantities of aqueous liquids very efficiently. On the other hand, if they are hydrophobic, or made of hydrophobic materials such as Teflon, negative capillarity effects can cause the liquid to not move until sufficient force overcomes the meniscus forces that cause it to stop. These properties are the basis of passive valves on microfluidic devices.

Hydrophobic valves are based on a restriction in a hydrophobic zone. The restriction causes a significant pressure drop and the disc must be spun at an angular velocity high enough to produce the centrifugal pressure to overcome that drop before the fluid will enter the channel. Equations 2 and 3 are generally accepted for predicting the pressure drop and the frequency at which the pressure is overcome and the valve bursts (i.e. starts to flow). This is known as the burst frequency.

$$\Delta P = 2\sigma_l \cos\theta\left[\left(\frac{1}{w_1}+\frac{1}{h_1}\right)-\left(\frac{1}{w_2}+\frac{1}{h_2}\right)\right]$$

ΔP = pressure drop
w_1 and h_1 = width and height before channel restiction
w_2 and h_2 = width and height after channel restriction
σ_l = surface tension
θ = contact angle at liquid - surface interface

Equation 1.2 Pressure needed to move fluid past rectangular channel restriction.

$$\omega_b = \sqrt{\frac{P_m\,(>\Delta P)}{\rho r \Delta r}}$$

$P_m > \Delta P$ at burst pressure
ω_b = burst frequency in Hz

Equation 1.3 Combination of equations 1 and 2 to predict the frequency at which a hydrophobic valve bursts.

These equations are independent of channel length and flow velocity. Only the restriction size, contact angle (σ_l)[39], and surface tension (θ) influence the burst frequency.[60,61] This makes valve construction relatively simple as all samples in a given analysis, even those with high degrees of matrix effects, generally have similar contact angles and surface tensions.

Hydrophilic valves, based on capillary action, will draw liquid into the channel but flow will not occur due to the barrier pressure created by the liquid's meniscus at a significant expansion of the hydrophilic channel. The barrier pressure for hydrophilic valves is extremely complicated and depends on the valve geometry and the liquid-air-solid interfacial properties. Ducrée *et al.* proposed Equation 4 to predict the burst frequency of a capillary valve.[63] However, it has been noted that the wedge angle, or angle the wall around the end of the capillary recedes at, and the aspect ratio of the channel can affect the burst frequency.[62]

$$\nu\,(Hz) = \frac{1}{\pi}\sqrt{\frac{\sigma|\cos\theta|}{\rho r \Delta r d}}$$

ν = burst frequency in Hz
σ = surface tension
θ = contact angle at liquid - surface interface
(Θ used by author[63])
d = diameter of restriction

Equation 1.4 Predicted frequency needed for the progression of the meniscus across a capillary barrier.[63]

Other considerations in centrifugal microfluidic valving include deviations caused by imperfect valve shape due to small-size and rough surfaces that increase the degree of hydrophobicity or hydrophilicity. Samples that have very low surface tensions and/or tend to vaporize over the life time of the experiment are difficult to handle without an active valve. Active valves incorporated in discs are similar to the ones used on chips and are at a level of complexity not required for the experiments described herein.

There is some disagreement about the theoretical equations governing microfluidic valves. Several papers suggest that these equations are not limited to hydrophobic or hydrophilic samples as the interfacial properties seen with either type of material play a strong role in both predictive equations.[63,66] Only within the last few years have papers been published solely dedicated to studying these phenomena. A discussion of valving on microfluidic discs is also covered in Chapter 5.

1.5.6 Mixing

Mixing on conventional chip-based microfluidic platforms has presented a challenge due to the fact that the flow is generally laminar due to the small channel dimensions used. Because of this, most designs generally include long channels to allow time for diffusion-based mixing to occur. There are more efficient ways to ensure complete homogenization in centrifugal devices because of the fact that the discs are in motion. Rapid changes or even reversals of the angular velocity cause inertially-induced "twisting" or mixing of the liquid.[64] Externally induced agitation of on-disk magnets and micro-beads have also been used to provide more rapid mixing and as a means of cell lyses. This topic is also covered in more detail in Chapter 5.

1.5.7 Other Capabilities

Centrifugal microfluidic devices also have other capabilities such as: chromatography and solid phase extraction, siphoning, metering, volume splitting, and droplet generation. These topics are covered more thoroughly in the literature[59,63,65-67] and were not required for the work described herein.

1.6 Conclusions

The levels of anthropogenic nitrogen in the natural environment have greatly increased in recent decades causing both positive and negative effects on human, wildlife, and environmental health. Due to the complexity of the nitrogen chemical cycle there is a pressing need to study both the cycle as whole, and the individual parts of the cycle. Nitrate and nitrite have significant effects on human health, specifically in their relation to water and wastewater sources. Hexavalent chromium, nitrate and nitrite are also ideal candidates for demonstrating the efficacy of emerging technologies such as the field of microfluidics. Centrifugal microfluidics has several potential advantages over conventional chip based microfluidics, primarily by inclusion of complete sample preparation and detection directly on a single disc. There is a need for the development of a centrifugal microfluidic device for the detection of nitrate and nitrite in water and wastewaters that is portable, simple to use, and both precise and accurate.

1.7 Objective

The objective of this research was to combine the disciplines of environmental science, centrifugal microfluidics, and spectroscopy to construct and characterize a complete method for the detection of the environmentally important chemical species of nitrate and nitrite. The detection of hexavalent chromium (Cr^{6+}) was also investigated to demonstrate that other single step reactions are easy to implement and to show the diversity of applications for this device on other environmentally important analytes. This thesis will demonstrate that centrifugal microfluidics are versatile and that the design and measurement methodologies presented here are adaptable to a wide variety of classic spectrometric analyses.

Chapter 2

INSTRUMENTATION

2.1 Rapid Prototyping of Centrifugal Microfluidic Discs

There are currently a variety of methodologies employed to fabricate microfluidic devices. Typically, either glass/Si/SiO_2 or poly(dimethylsiloxane) (PDMS) is used as a substrate for micro-fabrication with the microfluidic structures created in or directly on the material by photolithography or micro-machining.[71] These techniques work well for some applications as they use silicon materials which provide a larger range of optical transparency, can be performed in the laboratory, and have high feature resolution capabilities (approximately 30nm). Alternatively, soft lithography-based methods, which use elastomeric stamps or molds, can be employed to create the microfluidic structures.[72] The devices are then completed by bonding two, or more, layers together with anodic or fusion bonding.[73] Both photolithography and soft lithography have several drawbacks including the use of caustic chemicals and long baking times. Additionally, the use of photomasks, or negative masters in the case of molding, makes changing the design of the micro structures difficult and expensive rendering these techniques less than ideal for rapid device development.[74]

The micrometer (or smaller) scale of traditional, high resolution fabrication techniques may not always be required for many microfluidic applications where sample size is not limiting. Additionally, the smaller channels can become clogged with particulate matter seen in non-ideal, "real world" samples. Nanoscale fabrication techniques can also be quite expensive due to the high cost of the microfabrication

equipment, the need for dedicated clean room facilities, and extensive training needed by the operators. Furthermore, these techniques are not readily available to all laboratories. The frequent need to adjust or improve the design of microstructures has presented the need for novel rapid prototyping techniques. Thus, it was decided that a relatively new fabrication technique would be employed to facilitate rapid prototyping of centrifugal microfludic devices.

All of the microfluidic discs described in this work were fabricated using sub-millimeter resolution computer numerical control (CNC) machining combined with a simple, in-laboratory method known as xurography. Xurography is a digital production technique that uses a sharp blade to precisely cut, or "razor write", a thin sheet of varying thickness and composition. Several sheets are then layered and sealed together to make the final device. The method was first described by Bartholomeusz *et al.*[74] who used a CNC xurographic cutter produced by Graphtec America, Inc (model FC5100A-75; Santa Ana, CA). This xerographic device is capable of a cutting resolution of 10μm, but the instrumentation used herein was limited to a resolution of 200μm. Xurography is faster, has a cost advantage, is straightforward to learn, and is more adaptable than other rapid prototyping techniques, making it an ideal solution for prototyping microfluidic devices to work on the scales required for environmental analyses.

Many materials can be used with xurographic-based techniques; from surfaces specifically designed for reactions to inert materials that do not interfere with reactions. Small aspect ratio features on microfluidic devices, such as detection or reaction chambers, can be made in thin (100 μm) to thick (1 mm) material using either CNC xurography or milling. The thin, inert adhesive material used to bond the layers together

also provides a means of making the high aspect ratio features, such as channels or packed columns.

2.2 Device Fabrication

An overview of the complete process for disc fabrication is shown in Figure 2.1. The starting components were commercially available, uncoated polycarbonate discs available in two different thicknesses: a 1200 μm thick disc used in the manufacture of compact discs (CD) and a 600 μm thick disc used in the manufacture of uncoated digital video discs (DVD) (U-Tech Media Corporation, Taiwan). The 1200 μm thick disc was used as an internal layer that provided the depth, and hence volume, for the solution reservoirs. The top and bottom layers/covers were made using the 600 μm thick discs. The reduced thickness of the top/bottom layers reduced light attenuation by the discs and the overall thickness. The final, combined disc had a functional optical transparency to a low wavelength limit of about 350 nm.

A three dimensional engineering software program, SolidWorks 2005 (SolidWorks Corporation, Concord, MA), was used to design the disc and adhesive layer patterns. The disc layer patterns were subsequently transferred to a QuickCircuit 5000 computer controlled x-y-direction CNC milling machine (T-Tech Inc, Norcross, GA) to mill the 1200 μm thick polycarbonate disc layer. The cutting depth (z-direction) was manually controlled in instances in which it was not desired to completely mill though the disc. The adhesive layer patterns were transferred into Adobe Illustrator 10 (Adobe System Incorporated, San Jose, CA) prior to being sent to a CE3000-60 cutter/plotter (Graphtec America, Inc, Santa Ana, CA) for xerographic cutting of the adhesive film. For

all experiments described the adhesive layer was a 50.8-μm thick polyester film with a 25.4-μm layer of Flexmark® V-95 pressure sensitive acrylic adhesive on either side of the film for a total thickness of 101.6 μm (FLEXcon, Spencer, MA). For ease the adhesive is often referred to as 100 μm and will be in this work. Both sides of the adhesive were covered by a protective release layer until disc assembly.

After the adhesive layers were cut, the features (such as chambers or channels) cut into the release and adhesive layers were manually removed using a razor. An alignment hole along with a center hole was drilled or cut into all layers was used to insure proper (2 point) alignment of the discs and adhesive layers (Figure 2.1D-F). The 1200 μm thick disc had an extruded storage separation ring that had to be milled out for proper sealing of the discs. Once the disc was assembled it was sealed by the adhesive layers by cold pressing with a Sidewinder roller laminator (Desert Laminator, Palm Springs, CA).

The disc used for all of the Signal-to-Noise (S/N) data (see Chapter 3) was a simple design with 26 individual cells with injection holes but no channels or valves (Figure 2.2A). This design was chosen for maximum usage of disc space and permitted the many replicate measurements needed for S/N experiments. Discs used for the detection of nitrite and chromium (see Chapter 4) were similar to those used for the S/N experiments, except that a pellet containing all the reagents needed for analysis was inserted into the disc before the top layer was added and sealed (Figure 2.2B). The total pathlength for spectroscopic measurements was 1403.2 μm (a 1200-μm thick disc with a 101.6-μm thick adhesive layer). Due to variance in disc construction and sealing, however, the figure is most likely only accurate to 2 significant figures (1400 μm).

For the disc employing capillary valves (see chapters 5 and 6), multiple trial designs were made before the final model of the disc was designed. The original discs using capillary or hydrophobic valves were cut directly in the adhesive (Figure 2.3) and did not operate correctly. Hydrophobic surface modifications are explained in Chapter 5.

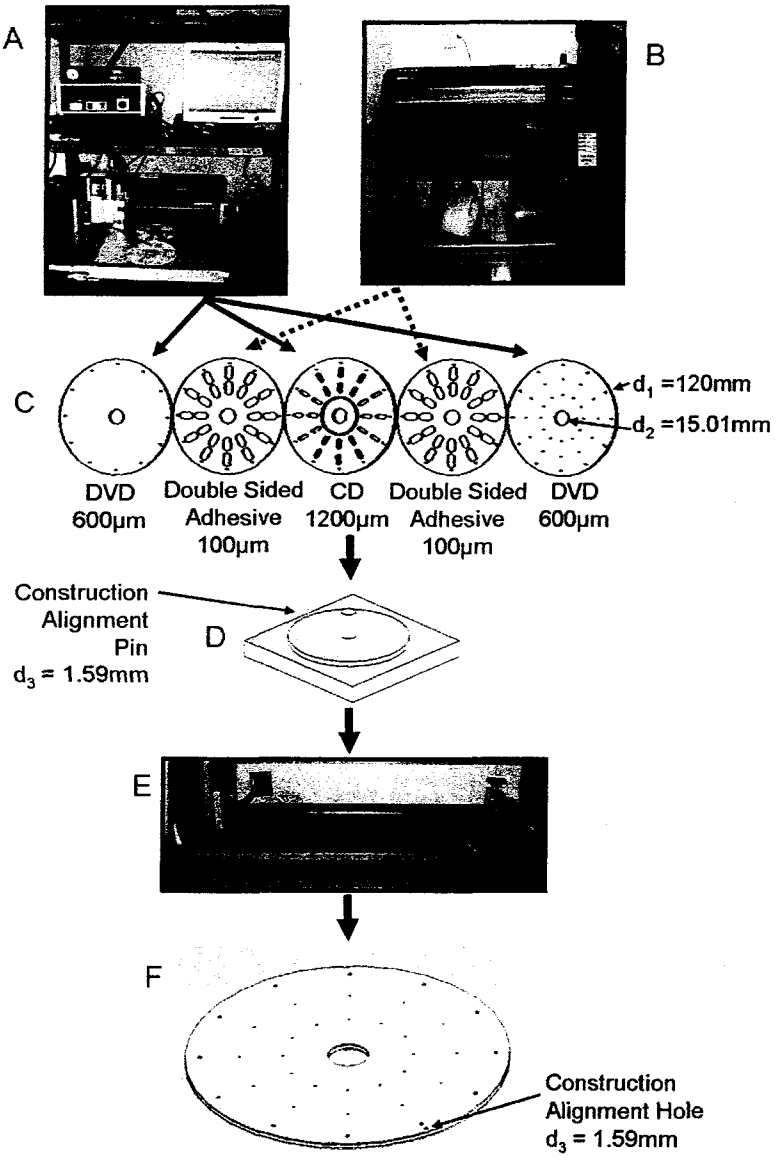

Figure 2.1 Construction of discs in the laboratory using a CNC milling machine (***A***) for small aspect ratio/millimeter scale features and a plotter cutter (***B***) for making large aspect ratio/micron scale features in inert pressure sensitive adhesive material (***C***). The individual layers (***C***) are carefully assembled using an alignment stage and alignment hole drilled or cut into each layer, then (***D***) cold pressed (***E***) to seal the final disc assembly (***F***).

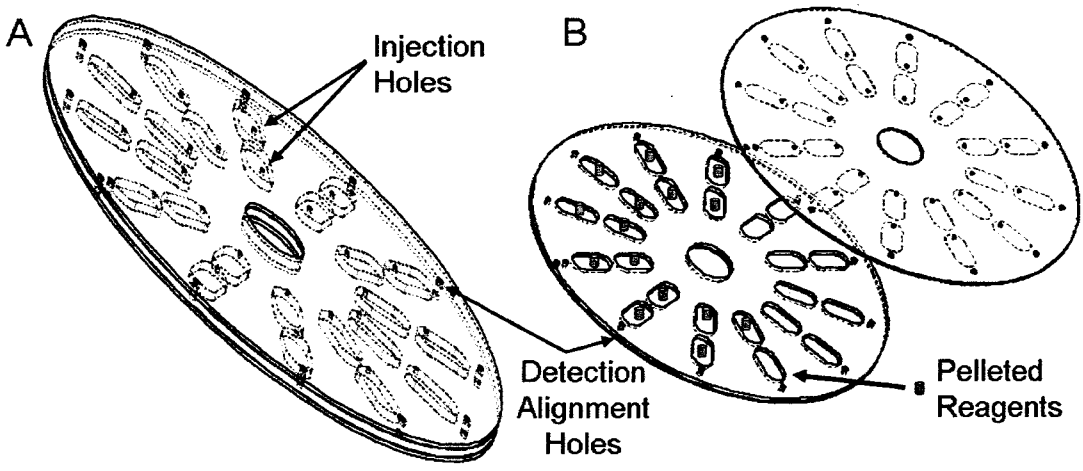

Figure 2.2 Disc model for all S/N measurements with 24 measurement cells (***A***). The same disc with pressed pellets added before the upper layer was sealed for use with one-step reagent systems (***B***). Discs are shown with hidden edges in grey dashed lines.

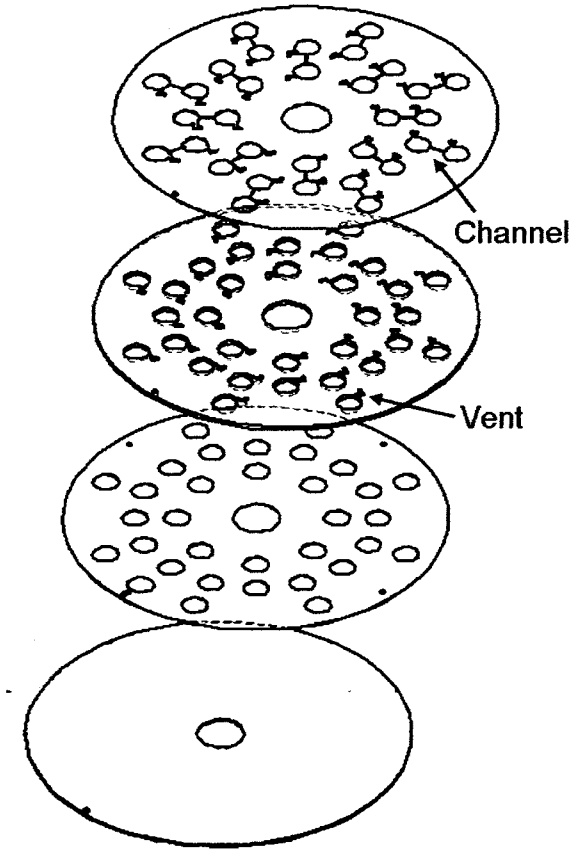

Figure 2.3 Centrifugal microfluidic disc used for capillary action and hydrophobic constriction valves made directly in the adhesive layer. For capillary action experiments the valve is on the bottom (outside) of the channel. For the hydrophobically modified discs, the valve is on the top (inside) of the channel.

A second type of valve was made by epoxying a quartz capillary (of various configurations) into a 1 mm wide x 1 mm long channel connecting the upper and lower chamber on the top side of the disc (Figure 2.4A). While the epoxy was still soft, the top layer of the assembly was added and any excess epoxy was cleaned away from the back of the disc (Figure 2.4B). If necessary a pellet of reagent was placed inside as illustrated in Figure 2.2B before the last layer was sealed on (Figure 2.4C). The reasoning behind each design is discussed within Chapter 5 and 6.

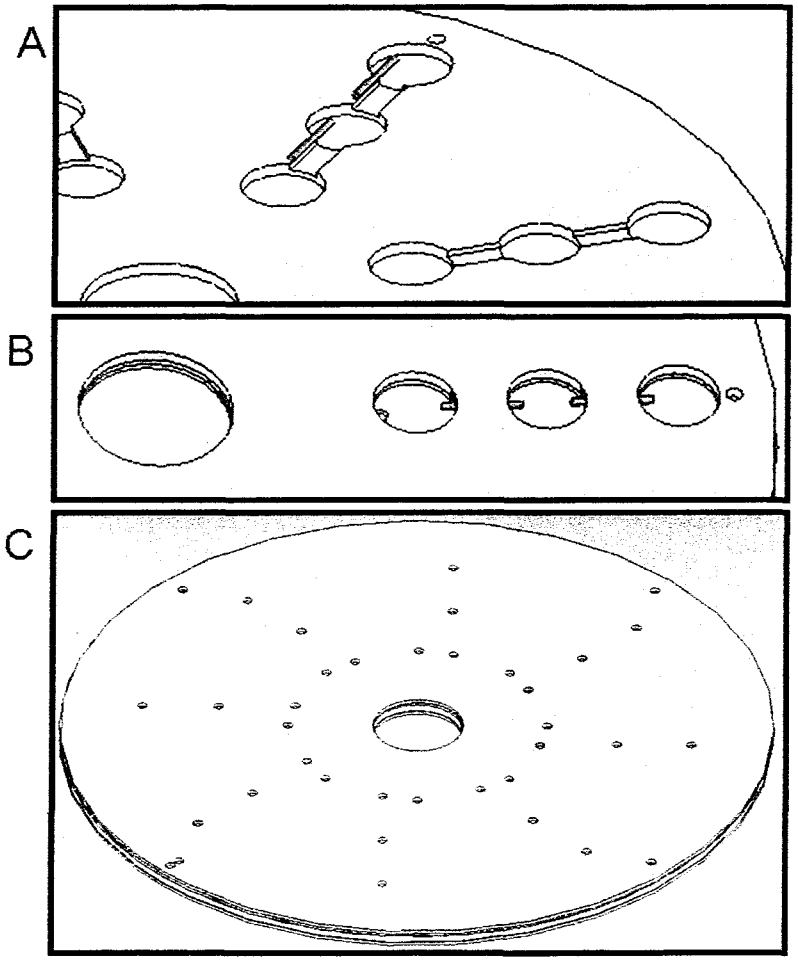

Figure 2.4 Construction of a centrifugal microfluidic disc with quartz capillaries used as hydrophilic valves (without pellets added). The epoxy resin is clear and is not shown. The vent is unseen as it is on the covered side in this representation.

2.3 Absorbance Detection System

Conventional, commercial spectrometer platforms are not capable of accommodating the measurements cells found on disc shaped microfluidic platforms. Thus, it was necessary to construct a custom spectroscopy system for absorbance detection.

The initial prototype absorbance detection apparatus (not shown) had several critical shortcomings. The entire apparatus was made of aluminium, which was responsible for scattered/stray light that interfered with the absorbance measurement. Additionally, the position and size of the light beam focused onto the disc was not adjustable. All initial experiments were performed on the prototype apparatus with a B&W Tek BTC111E spectrometer (B&W Tek, Inc., Newark, DE) which provided acceptable S/N ratios, but the software made the instrument difficult to control, and it was decided that a new detection apparatus should be developed and that acquisition of suitable software would benefit the project.

A second disc holder was custom built by the Technical Service Centre (Mr. Aldo Dissegna and Mr. Richard Alix, Concordia University), from a design schematic by Dr. Cameron Skinner and the author (Figure 2.5). It is adjustable in the x-y-z planes allowing for multiple thicknesses, sizes and disc designs. Two separate stabilization/alignment holes, which went through the entire disc, provided better stability and reproducibility in the disc placement (as indicated by arrows in Figures 2.1 and 2.2). The cut-away design allowed for the entire sample cell area to be free of reflective materials, reducing the amount of light scatter. A diaphragm was added between the collimating lens and disc to

adjust the size of the light spot, allowing multiple dimensions of detection chambers on the disc.

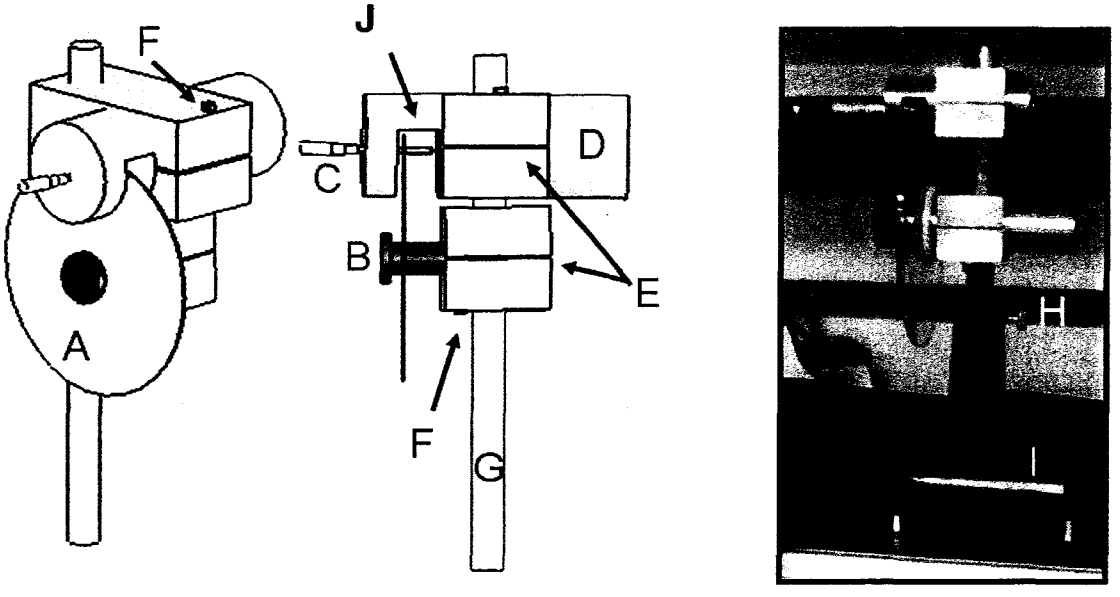

Figure 2.5 The disc (***A***) fits onto a cylinder fitted with a tightening screw (***B***) and is locked into position with a micrometer (***C***). ***D*** and ***B*** provide the X-axis adjustment by sliding through two blocks (***E***) that are fitted with tension screws (***F***). The blocks (***D***) also individually slide along ***G***, which provides movement along the Z-axis for different sizes of discs. Z-axis adjustment is also provided by adjusting ***H***, which allows the whole assembly to slide up and down. The entire apparatus is mounted on ***I***, which provides adjustment in the X-axis, using a typical optical rail mount. A portion of ***D*** has been cut-away (***J***) to allow proper positioning.

The final detection setup (Figure 2.6) was designed based on the practical usage of an earlier prototype along with comparison of several different commercial spectrometers (see Appendix A for data comparison). The detection apparatus design consisted of a Tungsten-Halogen/Deuterium light source with a shutter and separate power control for the two lamps (Ocean Optics, Dunedin, FL). The shutter provided the ability to obtain dark spectra without power cycling the lamp(s), thereby reducing the noise associated with lamp fluctuations. There was no wavelength isolation before the light reached the sample in the disc which allowed absorbance spectra to be collected by

the photodiode array spectrometer. The source provided continuum electromagnetic radiation in both the visible and ultraviolet range. The light source was coupled to the assembly using a 300 μm x 1 m, solarization resistant fibre optic (Ocean Optics, Dunedin, FL). The fibre optic was attached to the optical rail apparatus using a custom holder built by Mr. Fred Kluck (McGill University). The light was then collimated using a lens, directed through the sample (in the disc) on the disc holder apparatus described above, and focused onto the detection fibre optic connected to a USB4000 asymmetric crossed Czerny-Turner type miniature spectrometer with a linear charged coupled device (CCD) photodiode array detection system (Ocean Optics, Dunedin, FL) (Figure 2.6).

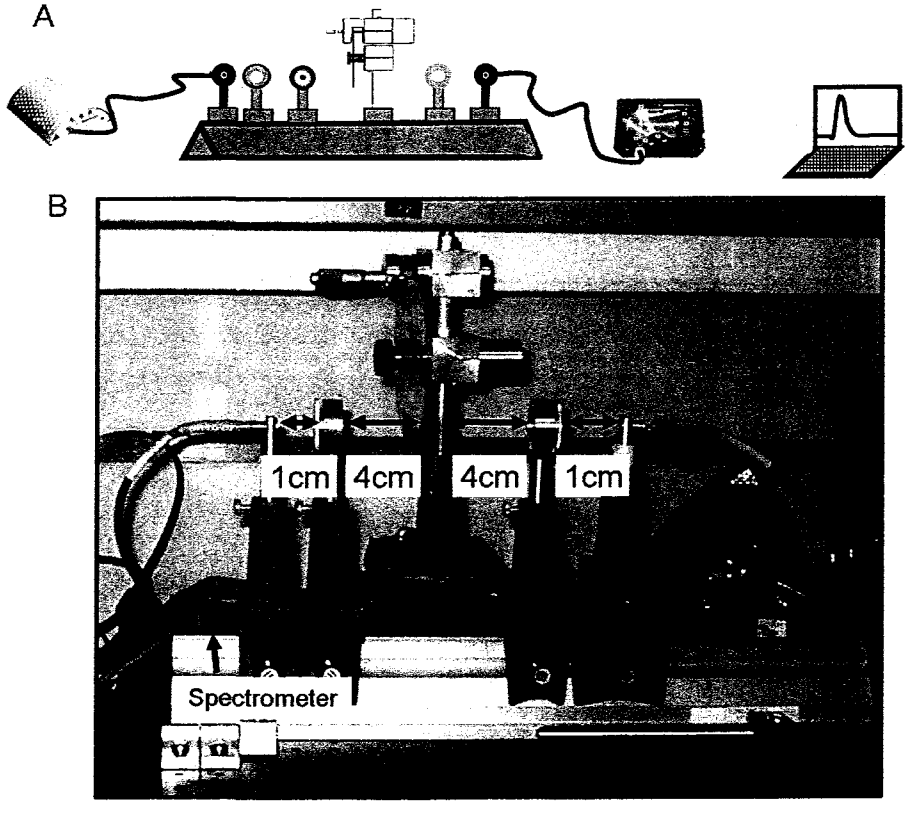

Figure 2.6 Schematic (*A*) of the portable system used for absorbance detection directly on the discs. From left to right: Light source, fibre optic, fibre optic holder, collimating lens, disc holder, focusing lens, fibre optic holder, fibre optic, spectrometer, USB cable laptop computer. Spectrometer and light source photos are from www.oceanoptics.com. Photo (*B*) of the system as used in laboratory.

The specifications for the spectrometer system and apparatus are listed in Table 2.1.

Table 2.1 Specifications of the centrifugal microfluidic absorbance system.

Component	**Description**
Fibre Optic Connections	SMA
Grating	600 lines / mm
Blaze Angle	400 nm
Wavelength Range	200-850 nm (200-850 nm filter)
Slit width	100 μm
Detector	DET4-200-850, 16 bit CCD linear PDA
Visible Range Resolution	1 pixel = 0.2 nm
Operating Software	SpectraSuite
Light Source	DT-Mini-2-GS
Fibre Optics	300 μm x 1m, solarization resistant
Collimating Lens	1 cm focal length, 25 mm diameter, BK7
Focusing Lens	1 cm focal length, 25 mm diameter, BK7

Chapter 3

INSTRUMENT SIGNAL-TO-NOISE CHARACTERIZATION

3.1 Introduction

Once an analytical instrument is constructed, it must be characterized as to how precise and accurate the measurements are that it produces. Instrumental noise causes fluctuations in the measurement of the analyte and reduces the accuracy and precision of the measurement.[75] It is important to differentiate error due to noise, which is random fluctuation within a signal, and error due to background, which is predictable and can be mathematically corrected for. The ratio of the average signal measurement compared to the standard deviation within that signal measurement is known as the signal-to-noise (S/N) ratio and is the inverse of the relative standard deviation. The S/N provides a useful way of identifying and reducing noise, with the goal of increasing the precision. There are several categories of noise, some of which will be discussed below, and there are many causes ranging from instrument design to chemical fluctuations. This study aims to find the main causes of noise in the prototype absorbance spectrometer system and describes methods to eliminate or reduce them in order to obtain the most precise measurements. The accuracy of the measurements will be discussed in later sections for each individual analyte.

Deviation within a given signal can be grouped into two general categories: fundamental noise and non-fundamental noise. Fundamental noise is random or "white noise" and comes from deviations in the system that can be characterized with mathematical equations. This type of noise is often referred to as Schottkey noise.[75] There

are many types of Schottkey noise, but two particularly important ones for this system are quantum noise and Johnson noise. Quantum noise arises from the fundamental nature of light. Quantum noise becomes important at low light levels such as those found in this absorption experiment at high analyte concentration levels. If quantum noise is a significant issue within a detection system, the S/N ratio will improve by the square root of the number of measurements taken.[75] Johnson noise follows this same pattern but is caused by electron carriers in conductors. It is generally not important if the total resistance of the electronic components is low. Furthermore, it can be effectively reduced by cooling the electronics systems.[75]

Non-fundamental noise can be random or non-random and is caused by imperfections or fluctuations within the instrumental and chemical system. Non-random noise, such as interference noise, can generally be found quite easily. An example is a spike at 60 Hz caused by power line radiation. Pink noise is a type of non-fundamental noise that is either random or non-random and is often referred to as flicker noise. It is seen in the low frequencies (1/f noise) of a spectrum and is frequently caused by lamp drift in absorbance measurements. Non-fundamental noise is often difficult to eliminate within a system. Excessive non-fundamental noise within a system can indicate a fundamental engineering problem.

3.2 Experimental

All experiments were done with a thick black cloth covering the entire absorbance spectrometer system along with the lowest ambient lighting possible in order to minimize stray light interference. The source lamp was allowed to run for at least 25 minutes prior to data collection to obtain the best stability. All data were recorded using the automatic

strip chart function built into the SpectraSuite Platform spectrometer software. All calculations were performed in Microsoft Excel spreadsheets using the raw data obtained from the spectrometer before any transformations to transmittance or absorbance were made. The final data was transferred into GraphPad Prism, where all error calculation and graphing was performed.

The signal-to-noise ratio is calculated by the following equations:

$$S/N = \frac{E_T}{\sigma_T}$$

Equation 3.1 Signal-to-noise equation.

Where:

$$E_T = \frac{\Sigma \text{Time Aqcuired Signal}}{n}$$

Equation 3.2 Average total signal.

$$\sigma_T = \sqrt{\frac{\sum x^2 - \left(\sum \bar{x}\right)^2}{(n-1)}}$$

Equation 3.3 Standard deviation calculation.

For the S/N calculations, a number of S/N measurements were made and then averaged and the deviation of the multiple measurements plotted. For both the single and multiple pixel experiments, the averages and errors were calculated from 20 sets of S/N data where each S/N set included 30 measurements.

All experiments except the initial S/N pixel experiment used the multiple pixel wavelength range shown in Figure 3.1. All experiments, except where noted, used a 10

second total integration time (TIT), with the majority using a 25 ms spectrometer integration time with 400 averages for a total time of 10 s. If necessary, the integration time and number of averages were adjusted to fit the data on scale, avoiding saturation, while keeping the total integration time constant. The total S/N was then calculated using the strip chart function for several concentrations of nitrite.

The absorption maximum at 508.12 nm (pixel 1577) was found to be the numerically highest absorption on a freshly made, midrange standard and was used in all the single pixel experiments. When multiple pixels were used, those corresponding to 499.13 - 540.06 nm (pixels 1532-1738) were chosen to use the entire flat part of the peak. Because the peak shifted with concentration and matrix, part of the peak shoulder was used. The majority of the sloped sides, where non-linearities from stray light and polychromatic radiation occur (Figure 3.1), were avoided.

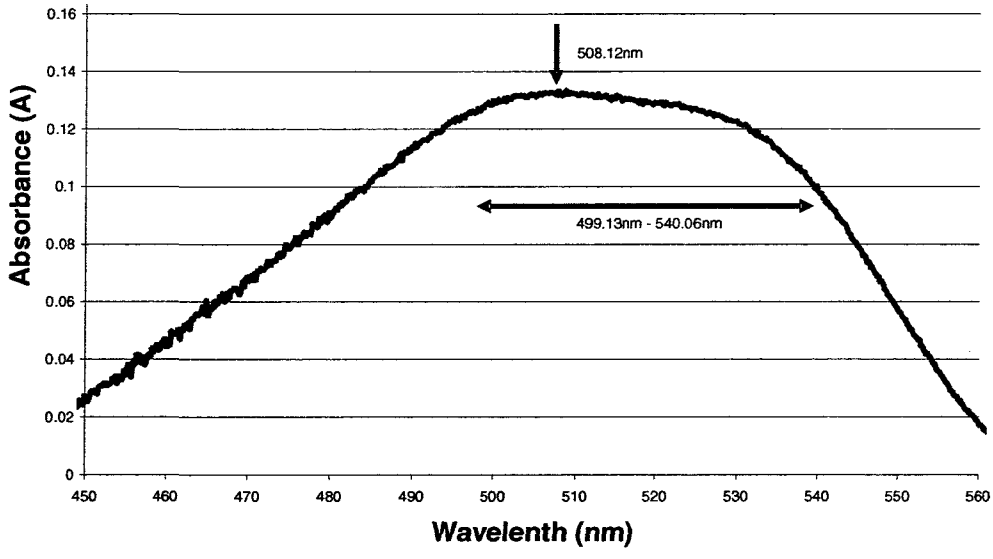

Figure 3.1 Absorbance spectrum of 0.5 mg L^{-1} nitrite-nitrogen complex using Nitriver3. Single wavelength (absorption maxima) and multiple wavelength regions used for calculations are highlighted.

3.3 Results and Discussion

By using the integrated signal from 499.13 - 540.06 nm there was roughly a 206 times increase in the use of the light hitting the detector when going from a single pixel to multiple (206) pixels. As stated above, Schottkey noise can be recognized by its characteristic $\sqrt{n}$ increase in the S/N ratio (the $\sqrt{206} \approx 14$). Using just one pixel for integration at the absorbance maxima for the nitrite test gave an average signal-to-noise ratio of 508. When using multiple pixels there is a 16 times increase in the average S/N ratio to 8074 (Figure 3.2). This suggests that random noise, as compared to lamp flicker noise, may be a factor associated with the detector pixel elements, as 16 is close to the value of 14 expected from theory. This experiment assumes a stable sample at one concentration and no extraneous noise sources. The variation in the S/N ratios probably arises because multiple wavelengths were used each with their own S/N. Because there is such a large increase in the S/N ratio using multiple pixels, all future experiments used multiple pixels for detection.

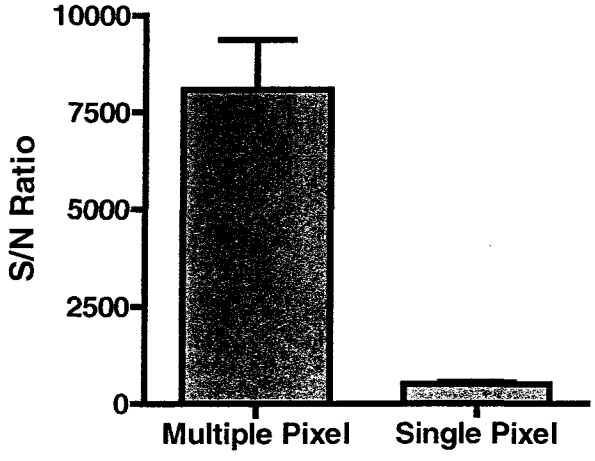

Figure 3.2 The average signal-to-noise ratio of an Ocean Optics USB4000 photodiode array using a 1200 μm disc as a cell for the detection of nitrite at 508.12 nm or 499.13 - 540.65 nm, with a total integration time of 9000 ms. Error bars are one standard deviation.

To evaluate the effect of dark current the light input to the spectrometer was completely blocked and the S/N from the photodiode array was measured. There was a maximum of 1.2% increase in the individual raw signals over a time span of 45 minutes, with an RSD of 0.4% for the entire time span (Figure 3.3). The raw signal of the highest concentrations of absorbing molecules is greater than 20,000 counts (in 10 s), so a change of less than 65 counts in the dark signal over the entire 45 minute experiment was insignificant.

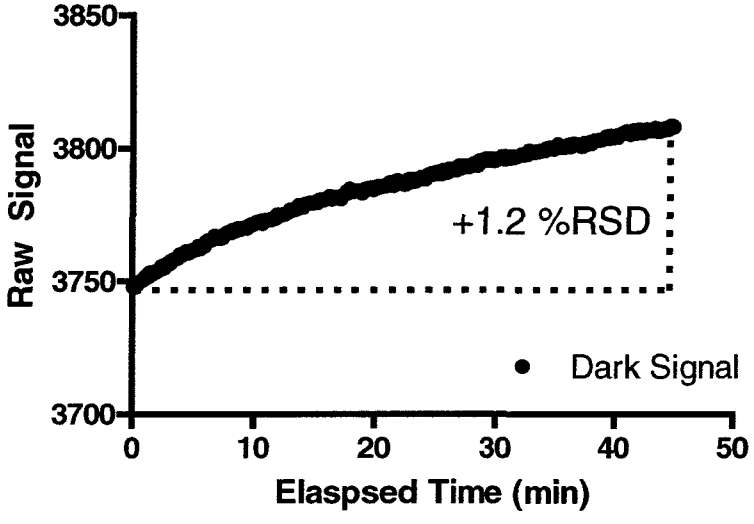

Figure 3.3 Raw signal of spectrometer output with all light blocked over (dark signal). Integration time was 9000 ms.

The same experiment was performed with no light attenuation and an empty disc cell in the light path. The results showed a much higher intensity but the change in the raw signal was only 367 counts, greater than the dark signal, but still not significant (Figure 3.4). An RSD of 0.24% over 45 minutes (Figure 3.4) was observed, indicating a highly stable light source. Typical analytical measurements were carried out in less than 45 minutes and no detection experiments lasted longer than two hours. The preceding

data suggests there was no significant change in signal due to drift in dark current or lamp signal. If an experiment would require a significantly longer time range or higher precision, the drift could be compensated for by taking blank or reference spectra throughout the experiment.

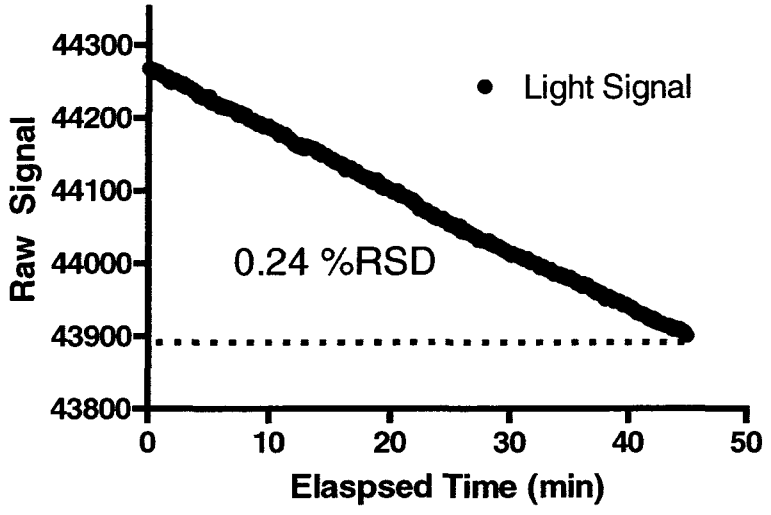

Figure 3.4 Change in raw signal over time for 100% transmission. The initial time point, zero elapsed time, starts 30 minutes after powering on the lamp. Integration time for each point was 9000 ms.

In absorbance, pink noise is often found at high light levels due to low frequency fluctuations in the lamp signal which is relatively large. Conversely, quantum noise can become precision limiting at high concentration levels where there is very little light to be measured.[75] To find the integration time with the highest precision throughout the concentration/light range, the S/N ratios for four different absorbances at several integrations times were found. Neutral density filters were used to provide a stable light flux corresponding to 0, 0.5, 1 and 2 absorbance units (A), instead of a solution that might degrade. The higher absorbances showed an increased S/N ratio at the higher integration time of 9000 ms (Figure 3.5). This was expected as shorter integration times

show less precision due to quantum noise contributions from the low levels of light available.[75] The lower absorbances showed lower precision at the highest and lowest integration time, with the best precision at the middle integration time of 900 ms (Figure 3.5). While longer integration times may show the fluctuations in the lamp signal caused by drift, the shortest might not be long enough to avoid quantum noise. The 9000 ms replicates showed similar S/N ratios compared to the 900 ms replicates at 0.5 A. The 9000 ms replicates also have a larger range of S/N ratios, suggesting that a total integration time of 900 ms gives about the same precision, is more reproducible, and saves analysis time (Figure 3.5).

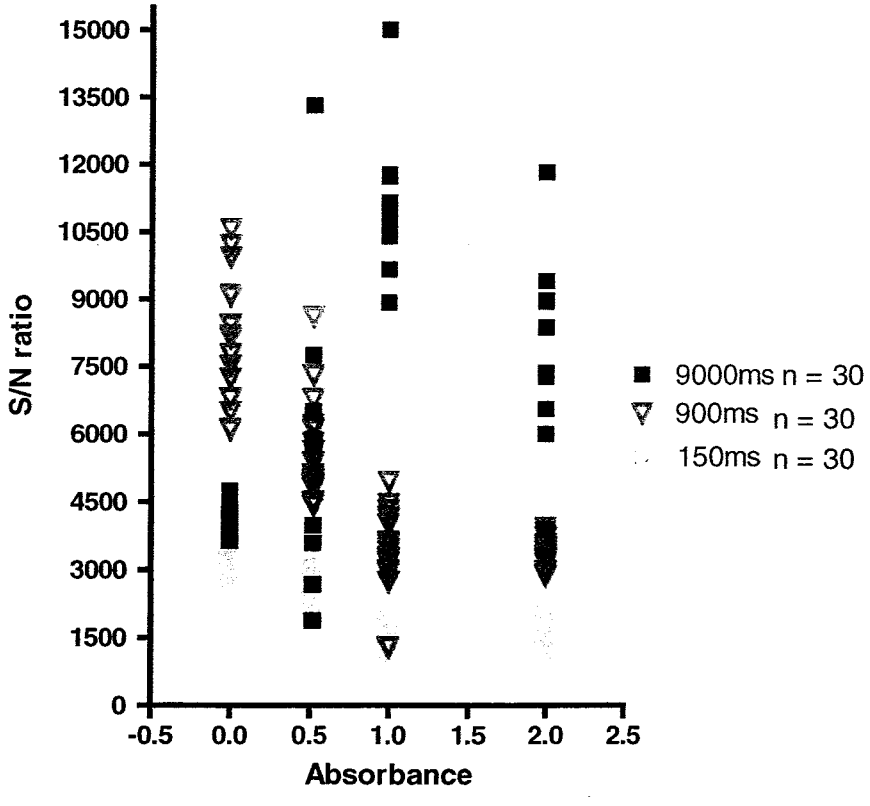

Figure 3.5 S/N ratios based on the amount of light absorbed and several different integration times. Each data point is the S/N ratio of 30 measurements, with 20 data points shown for each respective integration time. (Symbols offset to clarify data. Absorbances of 0, 0.5, 1.0 and 2.0 were used)

The spread of the 9000 ms total integration time (TIT) values is relatively large compared to the other integration times. The data in Figure 3.5 is taken from a single run of data obtained as a strip chart and then divided in to 20 sets of 30 measurements. Thirty measurements at 9000 ms is completed in about 270 s, while the same number of measurements at a 900 ms TIT is completed in about 27 s and 150 ms TIT in about 4.5 s, which is a significantly shorter time scale. The longer total time is takes to complete the 9000 ms data set may have introduced "false" noise into the system in the form of lamp drift. In order to look at the different integration times on a more realistic scale, the same data was rearranged to give 60 sets of n = 5 measurements (Figure 3.6).

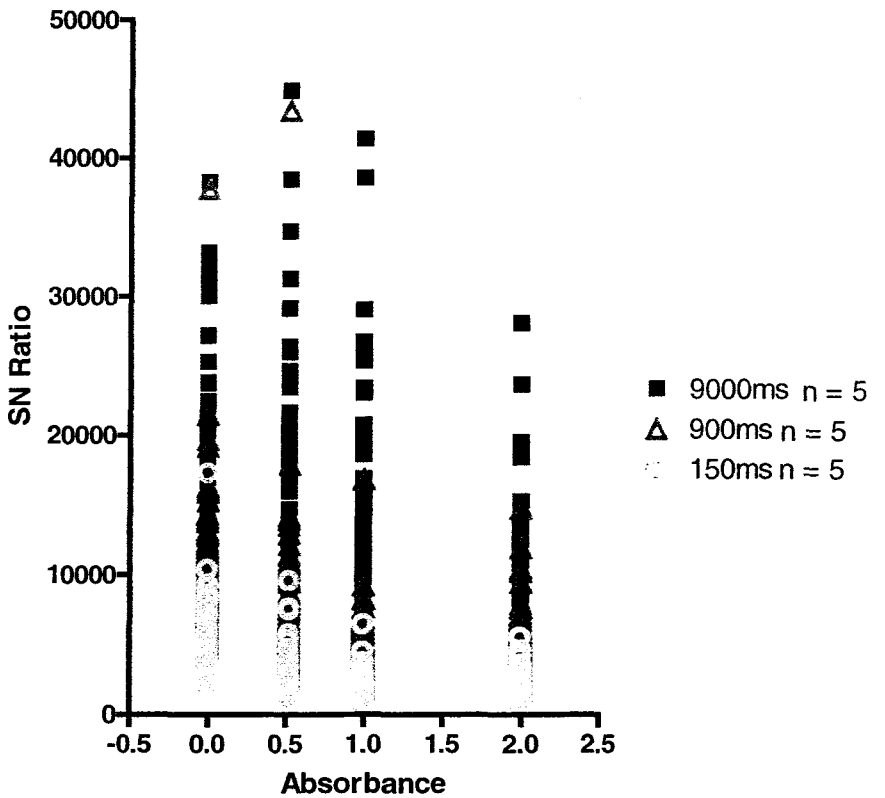

Figure 3.6 S/N ratios based on the amount of light absorbed and several different integration times. Each data point is the S/N ratio of 5 measurements, with 60 data points shown for each respective integration time.

Although this is a less statistically powerful way to analyse the data, it is more practical as the actual time taken for each sample is much closer to the time taken for 5 replicates than 20. It also reduces drift in the system that would appear over the longer time period. Decreasing the number of replicates per S/N ratio drastically increases the S/N ratio for all integration times and absorbances by greater than a factor of 3 (Figures 3.5 and 3.6). The S/N ratio has an increasing trend, with the best total integration time for all sample absorbances being 9000 ms. A total integration time of 10000 ms was also tested. The results were similar so a 10000 ms integration time was used for the rest of the samples due to ease of use.

The noise associated with the position of the disc caused the largest decrease in precision. There is 0.8 - 2 %RSD in the absorption measurements due to deviation in the blank and sample cells (Table 3.1). The inability to exactly replicate the placement of the disc on the disc positioning device is the most likely cause, as the disc positioning device does not return it to the exact same spot every time. There may have also been scratches or other imperfections on the disc itself causing scattering or local inhomogeneities in the absorptivity of the plastic.

Table 3.1 Deviation within absorbance measurements due to disc position (n =10).

Blank/Sample Pair	Average Absorbance	Relative Standard Deviation
1	0.0471	1.84%
2	0.0716	2.08%
3	0.0725	1.35%
4	0.0736	2.51%
5	0.0846	0.80%
6	0.1002	0.89%

Table 3.1 shows experiments in which the disc was re-positioned 10 times for both the blank and sample measurements. In normal experiments the disc is only positioned once for each sample/standard and all replicates taken from that position. Only the blank would be measured in multiple positions. Therefore, the relative standard deviations listed in Table 3.1 are greater than seen in most actual experiments.

3.3.1 Ratio Blank Method

In order to overcome the imprecision associated with the disc, a method utilizing an internal standard was used to estimate the blank. The classical equation for absorbance uses the transformation of transmission by a log function (Equation 4). Transmission is given by the amount of light (raw signal) at a certain wavelength(s) divided by the amount of originally available light (raw signal) at that same wavelength(s) (Equation 5). If multiple wavelengths are used, the average signal of the multiple wavelengths is used in the following equations:

$$A = -\log T$$

Equation 3.4 General equation for absorbance measurements.

$$T = \frac{I_{\lambda_1 Sample} - I_{\lambda_1 Dark}}{I_{\lambda_1 Blank} - I_{\lambda_1 Dark}}$$

Equation 3.5 General equation for transmission of light through a sample at a given wavelength(s) where λ_{etc} signifies the intensity measured at that wavelength.

Because of the inherent properties of absorbance measurements, the blank signal can also be estimated directly from the sample spectrum itself as long as the sample does

not absorb over the entire available spectral range. An estimate blank signal can be found by using a region of the sample spectrum where there is little or no absorbance. First, several sample spectra were taken and a wavelength at which the standards absorbs (λ_1) and one at which none of the standards absorbs (λ_2) was found. Second, a blank spectrum was taken. The ratio of the blank signal (I) at the samples absorbing wavelength (λ_1) to the blank signal at the samples non-absorbing wavelength (λ_2) was found (Equation 6).

$$Ratio = \frac{I_{\lambda_{1\,blank}} - I_{\lambda_{1\,dark}}}{I_{\lambda_{2\,blank}} - I_{\lambda_{2\,dark}}}$$

Equation 3.6 Ratio used in calculation for transmission from a single spectra

When a sample was run, the measured signal at the non-absorbing wavelength was multiplied by the ratio to give an estimated signal of the blank. For example, if the blank has a total signal of 10 units at the absorbing wavelengths and a non-absorbing wavelength total signal of 5 units, the blank signal is twice as great at the absorbing wavelengths than the non-absorbing wavelength. If the sample then has a non-absorbing wavelength total signal of 20, we can estimate the blank signal at the absorbing wavelengths would have been 40. When the entire calculations are worked out, the final transmission equation is as follows, with the absorbance equation remaining the same:

$$T = \frac{I_{\lambda 1\,analyte} - I_{\lambda 1\,dark} \Big/ I_{\lambda 2\,analyte} - I_{\lambda 2\,dark}}{Ratio}$$

Equation 3.7 Calculating transmission from a single spectrum (λ_1 is absorbing, λ_2 is non-absorbing) .

With a stable light source, a single blank spectrum can be taken and used to provide the ratio. This reduces the analysis time by decreasing the number of blanks taken and increases precision by avoiding the compounded noise in the blank signal. Because this was a prototype instrument the fiber optics were not permanently secured and the transmittance of different wavelengths of light through them varied based on the position of the fiber optic. Blank spectra were taken throughout the experiments to insure that the ratio was correct. Using the blank ratio method increased sample replicate precision (9 to 1 %RSD) and lowered the detection limit by an order of magnitude (0.09 to 0.008 1 mg·L^{-1}) for a nitrite curve performed on a centrifugal microfluidic disc (Figure 3.7 and see Chapter 4). All experiments after this chapter use the ratio method to calculate absorbance, unless noted.

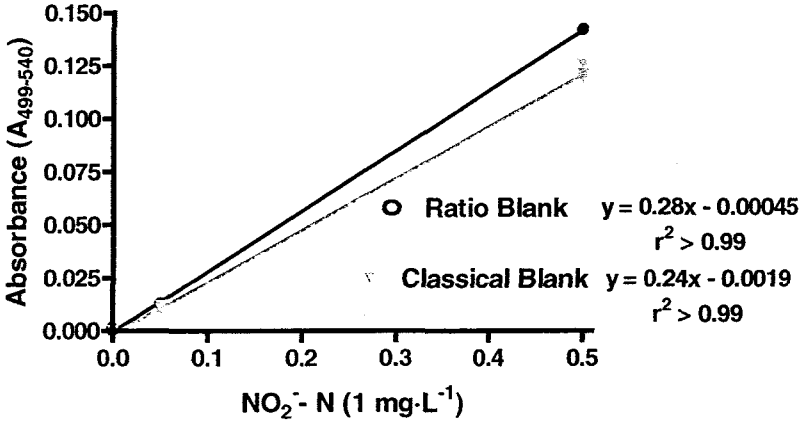

Figure 3.7 Comparison of classical and ratio blank for a nitrite-nitrogen curve using a microfluidic disc. (n = 3).

3.4 Conclusions

In the prototype absorbance detection system it was observed that there was noise due to drift in the dark and lamp signals, but the light source and detector are not the limiting source of precision. The deviation associated with imperfections and variations in the disc itself was the limiting noise factor. It is a non-fundamental noise caused by imperfections in the disc cells and (re-)positioning errors. In order to improve the precision of the system blank ratio estimation was employed. The best integration time for all concentrations was 9000 ms, with 10000 ms also being suitable. The absorbance detection system was suitable to work with many types of chemical absorbance reactions and proved capable of rapidly analyzing samples.

3.5 Future Directions

An experiment involving 400 and 100 pixels at different wavelengths compared to a single pixel could confirm that the detector is random noised limited if there is a 20 and 10 times increase in the S/N ratios, respectively. Mathematical analysis using a Fourier Transform (FT) at an appropriate sampling rate could be used to verify that the noise is random and shows no characteristic 1/frequency dependencey when plotted. It would also be useful to use several concentrations for this analysis. Cooling the detector could potentially lower any Johnson noise from the detector. The fibre optics should be secured to a permanent position when the system is used in the field to insure proper blank estimation when using the ratio blank method.

Chapter 4

SINGLE STEP REACTIONS: NITRITE AND HEXAVALENT CHROMIUM

4.1 Introduction

Two classic reactions were chosen for demonstration of single step spectrophotometric detection on the disc system: First, a modified Griess-Ilosvay reaction for the detection of nitrite (Nitriver3), second, the 1,5-Diphenylcarbohydrazide method (Chromaver3) for the detection of hexavalent chromium. Both reagents systems, Nitriver3 and Chromaver3, are commercially available from the Hach Company (Loveland, CO) that makes a wide range of simple field assay kits and reagents. These dry reagent packages come as a homogenous mixture containing all necessary buffers and derivatization reagents. In these experiments, sample injection, derivatization reactions, and detection were done in one cell on the disc. Hexavalent chromium and nitrite readily react stochiometrically with their respective dyes (Nitriver3 and Chromaver3), have derivatives with high molecular absorption coefficients. The systems are widely used and well characterized.[17,18,20,70] As in this introduction, each section below will begin with general information relevant to both of the single step reactions shown here and will be followed by sub-sections pertaining to the specific analyte.

4.1.1 Nitrite

The modified Griess reaction used in this work for the detection of nitrite has several intermediate species. A primary aromatic amine (sulfanilic acid) in an acidic solution forms a product (Figure 4.1, Step 1) which reacts with nascent nitrous oxide in the sample forming the diazonium ion (Figure 4.1, Step 2). The nitrous oxide is formed

from the nitrite in the sample. The diazonium ion then reacts with the chromotropic acid forming a highly conjugated colored product that readily absorbs from 499.13 - 540.06nm (Figure 4.1, Step 3).

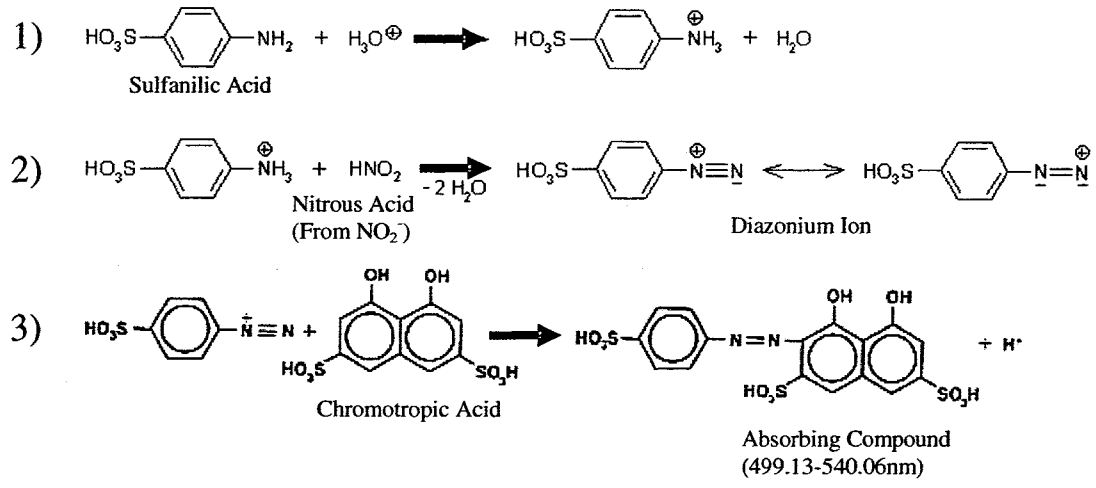

Figure 4.1 Modified Griess reaction used in Nitriver3 reagent system to detect nitrite.[78,79]

The absorbance maximum of the asymmetric absorbance peak is known to shift depending on the pH of the final solution. The maximum absorbance of the protonated form of the final product in the classical Griess reaction (see Chapter 1) is around 540 nm while the ionized form is around 500 nm.[76] The absorbance of the Griess reagent system is linear with concentration for any fixed wavelength and pH.[76] The modified Griess reagents in the Nitriver3 system are buffered at a pH of 3. For the reaction and concentration range used in this work, there is a slightly variable absorbance maximum dependent on the nitrite concentration with the average found to be 508 nm. The manufacturer's suggested measurement wavelength is 507 nm.[77] For practical concerns and better S/N ratios, all measurements on disc used a range of wavelengths (499.13 - 540.06 nm) that included the maxima of all concentrations used in this work.

The Nitiver3 system has several known interferences that could pose problems when used in complex matrices. These include interference by precipitation with divalent and trivalent ions (Sb^{3+}, Au^{3+}, Bi^{3+}, Fe^{3+}, Pb^{2+}, Hg^{2+}, Ag^{2+}, Fe^{2+}, Cu^{2+}, $PtCl_6^{2-}$, VO_3^{2-}). Furthermore, cupric and ferrous ions can also cause low results. High levels of nitrate (>100 $mg \cdot L^{-1}$ NO_3^--N) can undergo slight reduction to nitrite during the reaction period. Finally, strong oxidizing or reducing substances interfere at all levels.[77] None of these interferences caused a problem during the analyses described herein.

4.1.2 Hexavalent Chromium

The reaction of 1,5-diphenylcarbohydrazide with hexavalent chromium in an acidic buffer solution produces a red-violet color with a strong, broad absorption peak ($\varepsilon = 4 \times 10^4$ $L \cdot g^{-1} \cdot cm^{-1}$) with a maxima at 540 nm. The structure of the absorbing molecule is not well established but is generally believed[20] to be 2 dye molecules to 1 Cr^{6+} as shown in Figure 4.2. No known interferences were encountered; however, it is known that iron and vanadium levels above 1 $mg \cdot L^{-1}$ may interfere, and there is a slight interference from mercurous and mercuric ions. It is also known that highly buffered, extremely acidic or basic samples will exceed the buffering capacity of the reagent package and require pretreatment.[20, 80] The reagent is stable for long periods of time at room temperature but is unstable when it is exposed to high temperatures above 200°C.

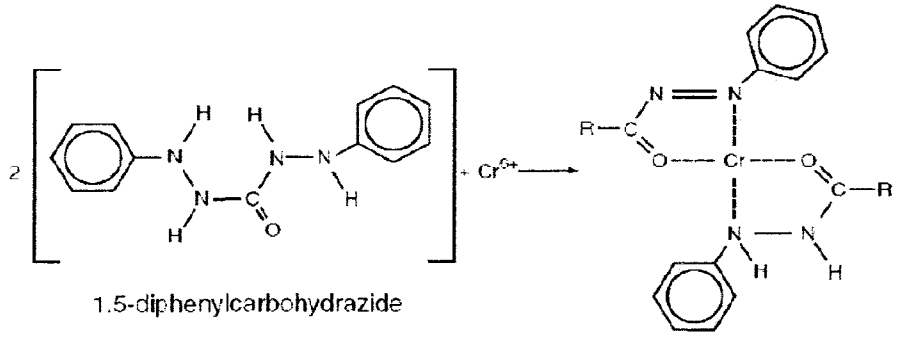

Figure 4.2 The suggested mechanism for reaction of hexavalent chromium with 1,5-diphenylcarbohydrazide.

4.2 Experimental

The reagents for both types of reaction were purchased from Hach Corporation (Loveland, OH) in the form of sealed foil and plastic "pillow packets". The declared reagents are listed in Table 4.1 but the actual mass of each component is not known. To assess the analytical performance and establish the experimental parameters to be used on disc (described in greater detail below) standards were measured using a common field test, standard spectrophotometric instrumentation, and two different ways using a microfluidic disc.

Table 4.1 Reagents included in each of the pillow packets used for the single step reactions.

Nitriver3®	**Chromaver3®**
Chromatropic Acid, Disodium Salt	Potassium Pyrosulfate
Sodium Sulfanilate	Magnesium Sulfate
Potassium Pyrosulfate	1,5-Diphenylcarbohydrazide
Potassium Phosphate, Monobasic	
1,2-Cyclohexanediaminetetraacetic Acid Trisodium Salt	

Initially, a common field experiment sold commercially by Hach was performed. The test consisted of 6 subjects evaluating the transmittance of six derivatized standard solutions in random order. The standard solutions were prepared according to the manufacturer's suggested protocol in an approximately ½ inch diameter, 15 mL tube. The intensity of the sample was then compared to a calibrated intensity disc.

The large scale experiment consisted of preparing standards and reagents according to the manufacturer's suggested protocol and measuring the resulting spectra with a bench top spectrometer (1-cm pathlength cell). A second set of standards made according to the suggested protocol were made and injected into an empty, clean disc (1.40-mm pathlength cell). This showed any problems caused by using the disc as a cell instead of a conventional bench top cell. The final experiment for each analyte was to make pellets containing a scaled amount of dry reagent for 100 µl of standard. The pellet was placed in the disc during construction as seen in Chapter 2 and in Figure 4.3. Powder was initially used, however, due to static forces the powder was dispersed around and out of the cell during the final disc construction step. To avoid modifying the reagent with a static reducer, a reagent pellet containing approximately half of the pillow packet contents was made using a pellet press. The large pellet was then broken into pieces with the edge of a razor blade. Static continued to scatter the small fragments, but this could be avoided if the disc top and bottom were wiped with ethanol before the disc was sealed. After sealing the disc, vinyl adhesive was used to seal the access ports/openings to the cell and the entire disc was placed in a desiccator until use. When an experiment was performed, 100 µL of standard or sample was injected into the disc and the seal was replaced. The disc was then agitated manually or mechanically until the pellet was

completely dissolved (Figure 4.3) (see chapters 5 for more detail on mixing). The disc was then placed in the custom spectrometer shown in Figure 2.4 and the absorbance measurement taken.

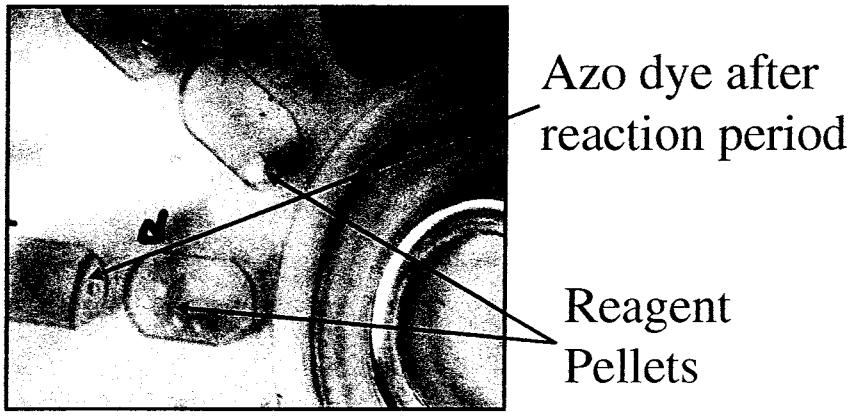

Figure 4.3 Disc used for the derivatization and detection of nitrite and/or hexavalent chromium using pressed powder regent pellets.

4.2.1 Nitrite

For all nitrite experiments, standard reference solutions containing either 1000 $mg \cdot L^{-1}$ nitrate (NO_2^-) (SCP Science, Baie D'Urfé, Quebec) or 100 $mg \cdot L^{-1}$ NO_2^- as nitrogen (NO_2^--N) (SPEX, Metuchen, NJ) were diluted serially by weight to an appropriate concentration of NO_2^--N with reagent grade water. For the large scale experiments, 5 mL of standard was placed in a 7 mL glass vial and the entire contents of a single pillow packet were added. The vial was capped and shaken manually for approximately 30 s or until the reagent was complete dissolved. The reaction was allowed to proceed for 20 min before measurement. Bench instrument measurements were made using a 1-cm optical grade, plastic cell from Ocean Optics (Dundin, Florida) and an Agilent 8453 spectrometer was used to take the absorbance measurements. The powdered reagents in

the pillow packet had an average mass of 0.153 g. The amount of reagent powder needed for each cell was 3 mg, but due to difficulties working with small amounts of material between 2 – 6 mg of material was placed in each cell. For the nitrite calculations, the average absorbance from 499.13 - 540.06 nm was used for the absorbing wavelength and 603.07 - 623.82 nm for the non-absorbing wavelength as described in Chapter 3.

A study was done to establish the length of time the pellet regent was stable and the effect of pellet size on absorbance. A single disc was constructed as normal, sealed and placed in a desiccator until use. A fresh solution of approximately 0.5 $mg \cdot L^{-1}$ NO_2^{-1}-N was made each day and the absorbance taken. The final absorbance was adjusted for any difference in standard concentration.

4.2.2 Hexavalent Chromium

For all chromium experiments, chromium standards were made daily from a 100 $mg \cdot L^{-1}$ $K_2Cr_2O_7$ solution (SCP Science, Baie D'Urfé, Quebec) in clean, 30 mL plastic bottles to the final concentration. For the large scale experiments the pillow packet was added to 10 mL of standard, and shaken until completely dissolved. Weighed reagent pellet fragments between 1.5 mg and 2.2 mg were placed on the disc. Contamination of the initial Chromaver3 pellets necessitated covering the metal surfaces of the pellet press with Parafilm or replacement with Teflon. All chromium experiments were allowed to react for 8 min prior to taking the absorbance measurement. For the large scale experiments, the 1-cm cell was made of optical grade plastic and an Ocean Optics cell holder and detector were used. Measurements on the disc were taken using the ocean optics spectrometer and the custom disc holder (see Figure 2.4).

Inconsistencies in fiber optic placement during the chromium (VI) experiments necessitated calculating absorbance data in the classic manner (not using the ratio method), using the averaged blank signal taken before and after each sample. Additionally, for chromium, the ratio method was used to calculate the absorbance data using 529.98 - 559.91 nm for the absorbing wavelengths and 757.92 - 785.98 nm for the non-absorbing wavelengths. Results were similar to the classical method, but provided higher detection limits and a lower replicate precision.

4.3 Results and Discussion

4.3.1 Nitrite

A widely used field method of detecting nitrite in water is to use the visual color comparison method mentioned in the experimental section above. The human eye is a log-normal detector and can discriminate a large range of colors and intensities, however, depending on the person, the color and intensity is open to subjective assessment.[81] This can become a large problem; for example, if the tester is color blind. This method was performed to show the limits of the currently accepted field methodologies and the need for an improved instrument. The method is appropriate for making decisions based on a sample concentration that is over or under a broad limit, but it is very imprecise due to differences in user eyesight and limited ability of the system to overcome differences in sample turbidity. Figure 4.4 compares the readings of six individual people to the actual concentration. This method has a limited working range from the detection limit of 0.1 - 0.5 $mg \cdot L^{-1}$ NO_2^--N and it has very poor accuracy at all levels of concentration (Figure 4.4). At concentrations greater than 0.5 $mg \cdot L^{-1}$ (the maximum comparison color that

appears on the disc) the error rises dramatically (and systematically) with an error of 50% at 1 mg·L^{-1} NO_2^--N.

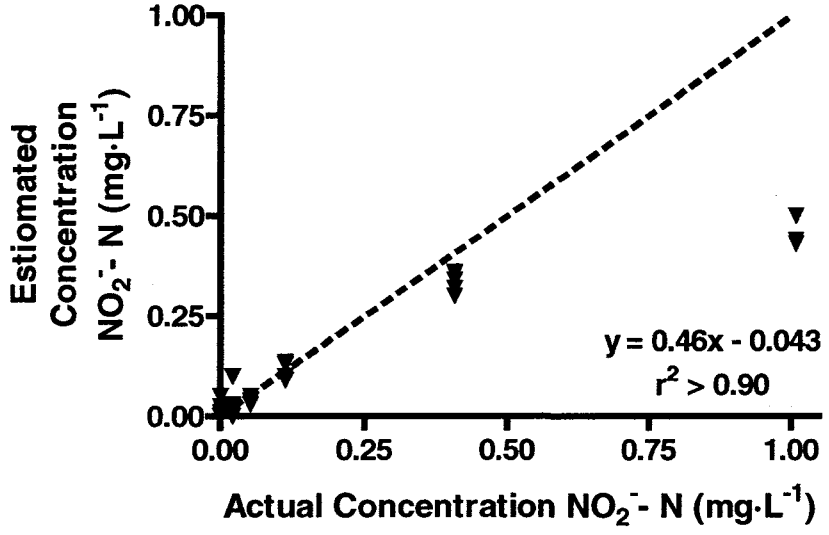

Figure 4.4 Comparison of standard concentration to visually estimated concentration using a conventional field analysis test kit, n = 5.

To increase the precision, accuracy and the dynamic range, field samples could be preserved and sent back to the lab for analysis using a bench top spectrometer. Using the Agilent HP8542 benchtop spectrometer with a 1-cm path length, the linear dynamic range was increased to 1 mg·L^{-1} NO_2^--N (Figure 4.5). The detection limit (DL) was lowered significantly to 0.006 mg·L^{-1} NO_2^--N and the precision improved to 1% for the 0.5 mg·L^{-1} standard (n=6). The 5 mg·L^{-1} and 50 mg·L^{-1} NO_2^--N standards were measured but did not follow Beer-Lambert's law for the wavelength range used (499 - 540 nm) and therefore are not shown on the linear calibration curve shown in Figure 4.5. Nitrite is easily converted to other nitrogen species during storage and environmental testing often uses a large number of samples. Accordingly, bringing samples back to the lab is not always an ideal analysis method.

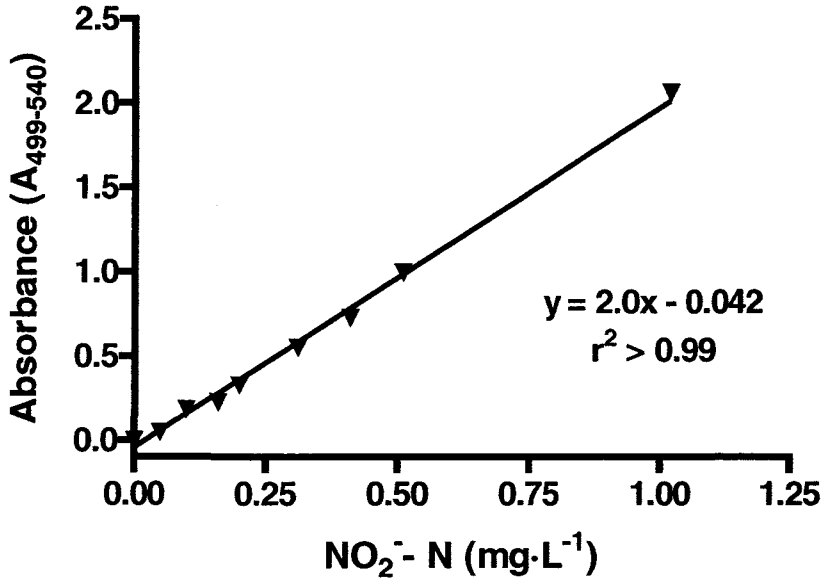

Figure 4.5 Detection of nitrite as nitrogen using conventional Nitriver3 pillow packets and a 1 cm plastic cell on an HP8543 photodiode bench top spectrometer (n = 3).

A calibration curve was constructed using the disc as a detection cell only and the customized disc holder with Ocean Optics spectrometer (i.e. bench top prepared standard solutions were injected to a clean prepared disc) in order to determine if using a microfluidic disc would affect the detection limit, sensitivity, and working range. The results were compared to those found using the standard bench top spectrometer above. The sensitivity was 0.26 A/mg·L^{-1} NO_2^--N which is close to the expected was 0.28 A/mg·L^{-1} NO_2^--N resulting from a 7-fold reduction in path length (Figure 4.6). The molecular extinction coefficient was approximately 2000 L/g·cm. The DL (0.009 mg·L^{-1} NO_2^--N) was almost an order of magnitude lower than expected based on the path length decrease alone. This is most likely due to cell placement noise.[75]

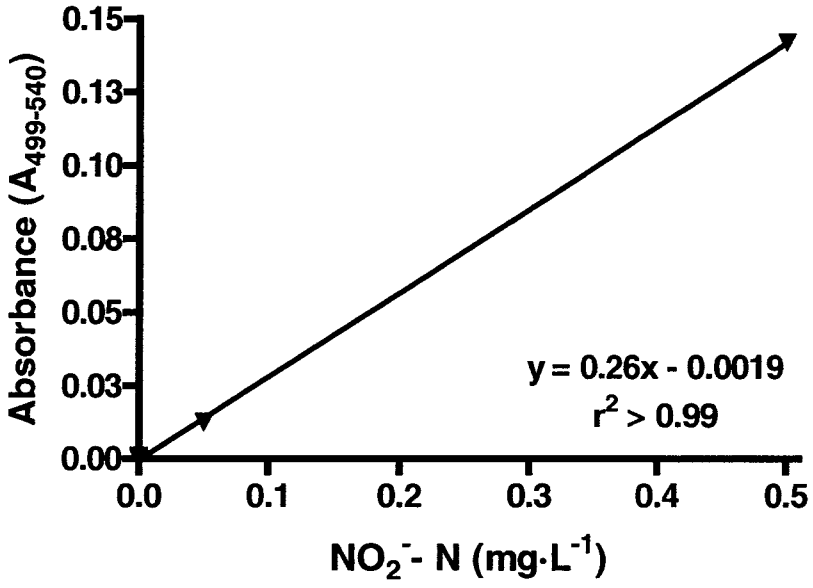

Figure 4.6 Detection of nitrite as nitrogen using Nitriver3 and a 1400-μm cell on a centrifugal microfluidic disc and the ocean optics spectrometer as shown in Figure 2.6.

It was noted during the experiment that the 5 mg·L^{-1} NO_2^--N standard was not linear when made using the standard protocol but was when excess Nitriver3 regent was added to the solution. This suggests that the 50 A/mg·L^{-1} NO_2^--N sample should have also been linear if reagents were in excess. As seen in the absorbance spectra in Figure 4.7, this was not the case in these experiments. The reason is unknown but may have a connection with the low light levels at 1.7A or that the 50 mg·L^{-1} NO_2^--N sample was noticeably more viscous than the other samples. The maximum linear absorbance value found in literature for all Griess reactions is 30 mg·L^{-1} [20,58], with the exception of regents specifically designed for high nitrite detection. No references where found with a large range involving a non-linear curve. For this reason a curve with an upper range of 5 mg·L^{-1} NO_2^--N will be used for further experiments.

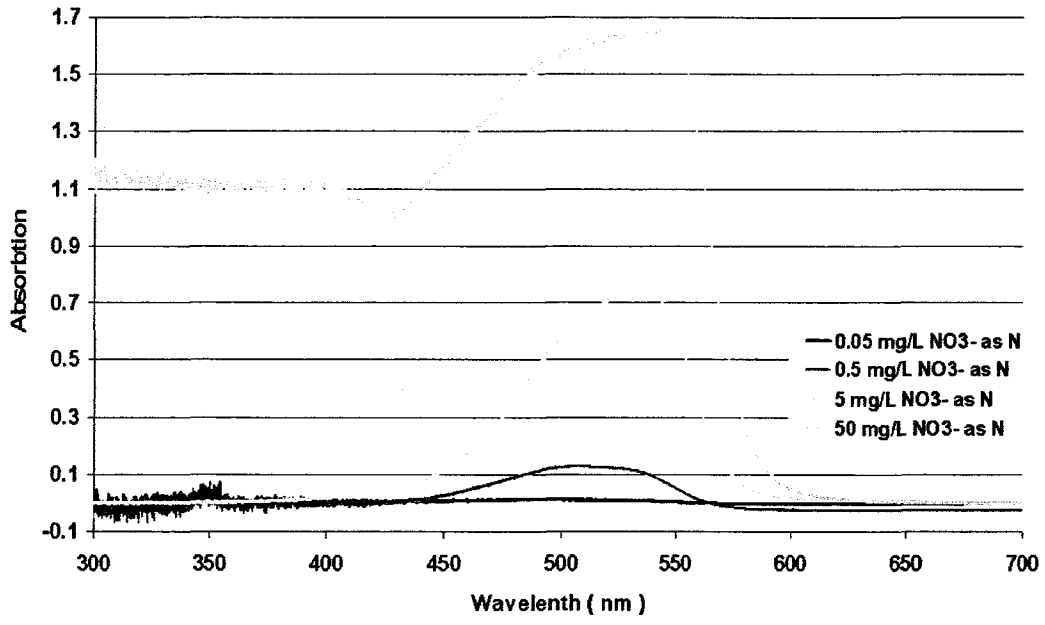

Figure 4.7 Absorbance spectra for nitrite-nitrogen when derivatized using Nitriver3 and a 1400-μm cell on a disc with Ocean Optics light source and spectrometer.

From these data, using the disc as a detection cell provided a means of keeping the detection limit and precision at levels comparable to those obtained with bench top instrumentation while lowering the needed sample volume to 100 μL and providing a portable disc size similar to the visual assay.

To verify that including the reaction and detection in a single step on the disc did not alter the analytical figures of merit a calibration curve using nitrite standards and pelleted reagent, as described in the experimental section above, was measured (Figure 4.8). The result was a linear curve ($r^2 > 0.99$) for the detection of nitrite-nitrogen with a slope of 0.27 A/mg·L^{-1} NO_2^--N and a detection limit of 0.008 mg·L^{-1} NO_2^--N. The slope and DL were comparable to those obtained when using externally prepared standards. The precision ranged from 0.2-3% RSD (n = 3-9) which is comparable to the bench top instrument. It was observed that small bubbles sometimes formed in some of the cells during reaction but could be removed by gently tapping the disc to dislodge them,

however, some remained causing light scattering and decreased precision. Table 4.2 provides a summary of the calibration parameters for the experiments listed in this section.

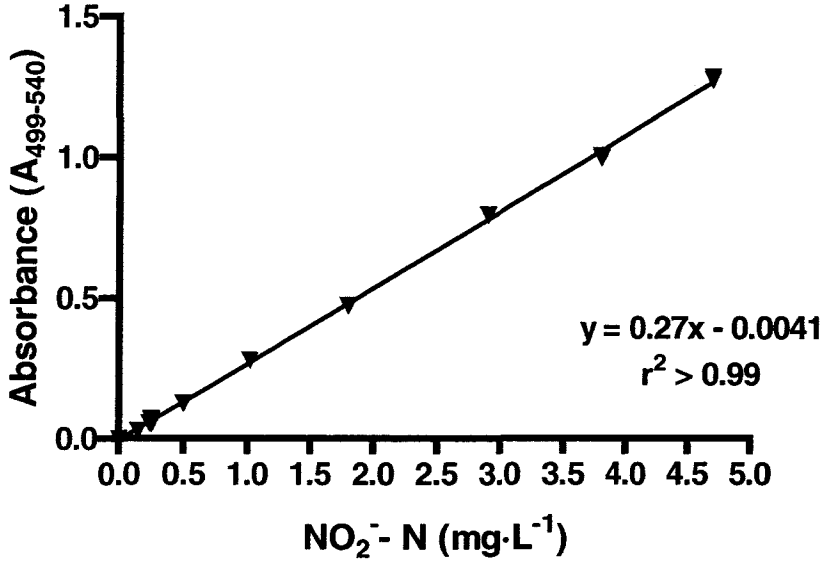

Figure 4.8 Derivatization and detection of nitrite as nitrogen using pressed Nitriver3 pellets and 100µL of standard (n = 3).

Table 4.2 Summary of calibration parameters for nitrite (NO_2^--N) experiments.

Test	Pathlength	Slope	DL	Upper calibration limit
Visual field test	0.5 in	N/A	0.1 $mg \cdot L^{-1}$	0.5 $mg \cdot L^{-1}$
Bench top instrument	1 cm	2 A / $mg \cdot L^{-1}$	0.006 $mg \cdot L^{-1}$	1 $mg \cdot L^{-1}$
Disc (as detection cell only)	1.40 mm	0.26 A / $mg \cdot L^{-1}$	0.009 $mg \cdot L^{-1}$	5 $mg \cdot L^{-1}$
Disc (complete)	1.40 mm	0.27 A / $mg \cdot L^{-1}$	0.008 $mg \cdot L^{-1}$	5 $mg \cdot L^{-1}$

A stability study was performed to determine how long a disc, with pellets included, could be stored and still provide reliable results. For the 31 day period tested,

there was no apparent trend (Figure 4.9). The daily % RSD between three different cells (the same solution in a single day) ranged from 0.8 - 2.7% RSD, showing that the individual cells are similar. Throughout the entire 31 day test period there was a 7.91% RSD in the concentration adjusted absorbance measurements with the measurements ranging from 0.29 - 0.38 AU. (i.e. the absorbance was adjusted for small changes in the standard solution which was made fresh daily) (Figure 4.9). This data shows that the method of making mg quantity pellets has the ability to provide a stable long term solution for a portable device. The reagents are known to be sensitive to water vapor in air.[77] Therefore, this data could be further improved upon with better sealing of the injection holes and storage of the disc in a desiccator.

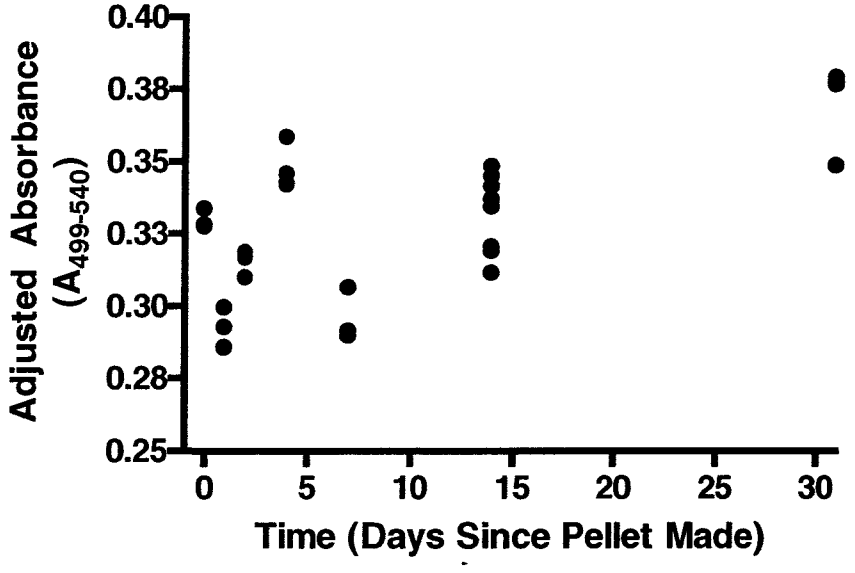

Figure 4.9 Adjusted absorbance for an approximately 0.5 $mg \cdot L^{-1}$ NO_2^--N solution injected into different cells over 31 days.

The stability study also provided a means of measuring the effect of pellet size on the absorption measurement. Figure 4.10 shows the same data as Figure 4.9 plotted

against pellet size. Again, there was no clear trend in the data. This suggests that pellet mass did not have a major effect on the absorbance of the solution. This is reasonable since the pillow packets are designed to provide an excess of reagents. So long as the pellet mass is large enough the on-disc reaction should also be with reagents in excess. It is important to note that this study was done over 31 days and that may have had an effect on the spread of the data.

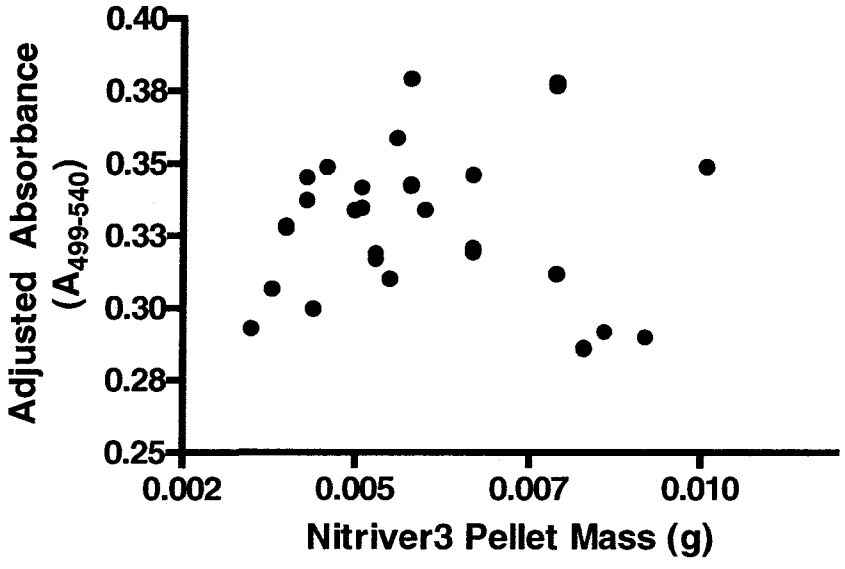

Figure 4.10 Adjusted absorbance of different sized Nitriver3 pellets over 31 days.

4.3.2 Hexavalent Chromium

As with the nitrite experiments the primary goal was to demonstrate that on disc derivatization and detection of hexavalent chromium was feasible. The visual test showed a linear trend for each individual person with an $r^2 > 0.98$ but when multiple users were combined the linearity decreased slightly to $r^2 > 0.97$ (Figure 4.11). However, the visual field method had poor accuracy with a systematic error of –30% (i.e. reported values were 0.7 times the actual concentration) and corroborates the results described in

Section 4.3.1 and Figure 4.4 for nitrite. Taken together, these results suggest that the current field methods using visual analysis are perhaps suitable for screening purposes only and are not precise or accurate enough for research or reporting functions.

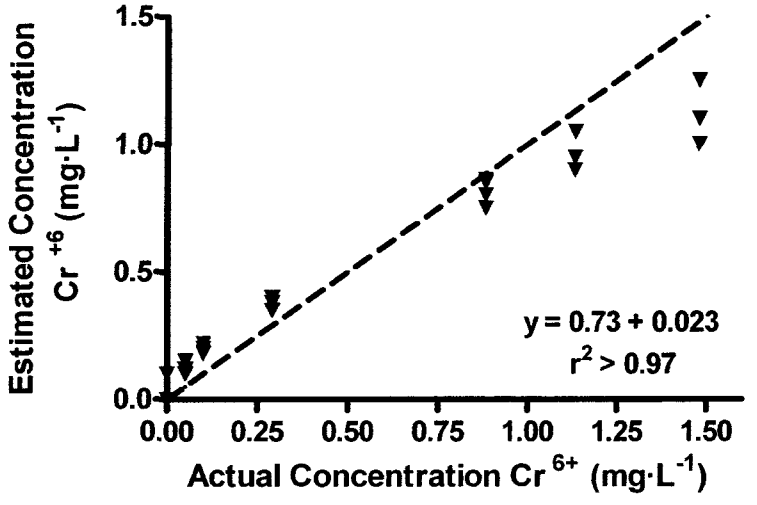

Figure 4.11 Determination of Cr^{6+} using a field method based on visual detection (n = 6).

To simplify the chromium experiments and result comparisons, only the Ocean Optics spectrometer was used (i.e. fiber optics were connected to either an Ocean Optics 1-cm cell holder or the disc holder). Using the manufacturer's recommended procedure (5 mL) and a 1-cm cell, a linear calibration curve from 0.02 to 5 $mg \cdot L^{-1}$ Cr^{6+} was found (Figure 4.12). The extinction coefficient (approximately 40,000 $L/g \cdot cm$ Cr^{6+}) and spectra shape closely agreed with literature[20, 70] (Figure 4.13).

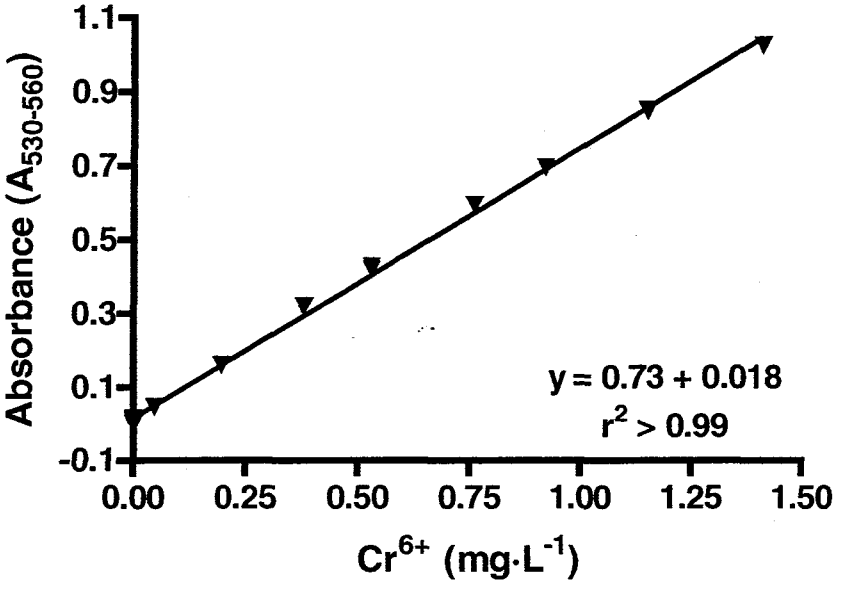

Figure 4.12 Average absorbance of Cr^{6+} standards using a plastic 1-cm cell (n = 3).

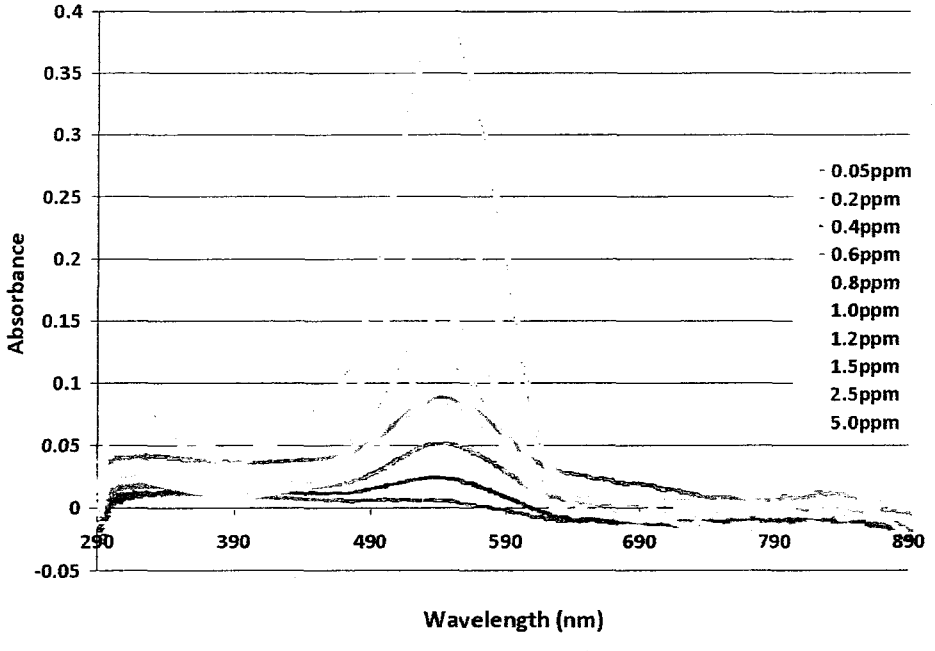

Figure 4.13 Absorbance spectra for Cr^{6+} using Chromaver3 derivatization and a 1-cm plastic cell.

Using externally prepared standards (5 ml) and a centrifugal microfluidic disc with a 1.40 mm pathlength as a detection cell, a calibration was performed. The calibration curve was linear from the detection limit at 0.04 $mg \cdot L^{-1}$ to 2.5 $mg \cdot L^{-1}$ Cr^{6+} and showed the expected slope of 0.099 $AU/mg \cdot L^{-1}$ Cr^{6+} (Figure 4.11). These results were particularly encouraging as the slope decreased almost an order of magnitude compared to the 1 cm path cell but the detection limit only increased by a factor of 2. Based on the absorbance of the highest standard the calibration curve most likely could have been extended as seen in Figure 4.16.

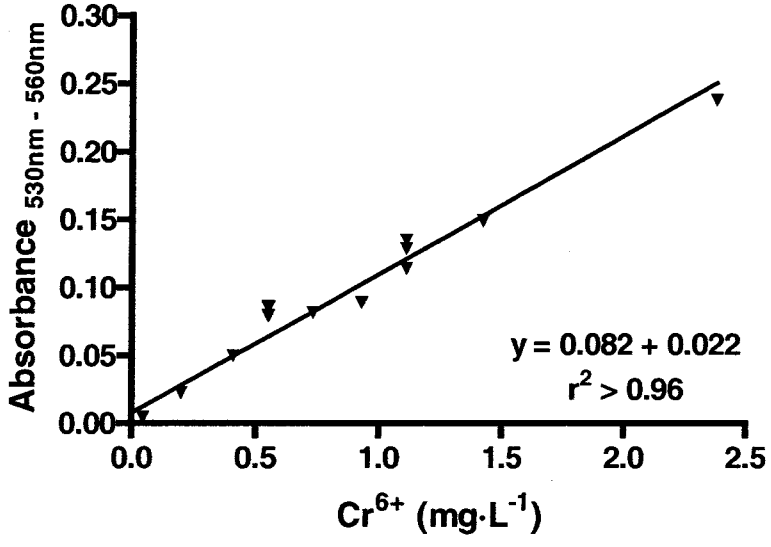

Figure 4.14 Externally prepared standards injected into 1400 μm disc and measured using the Ocean Optics and fiber optic spectrometer setup as shown in Figure 2.6.

Appropriately sized pellets of Chromaver3 were prepared and inserted into the disc during construction as described in Section 4.2.2. In some pellets a small amount of black material was transferred from the press onto the pellet surface. If this was seen the pellet was discarded. Even with this precaution, the resulting spectra were distorted with variable baselines and odd absorbance features over the entire spectrum (Figure 4.15A).

The three highest chromium concentrations showed normal spectra except for the altered baseline (Figure 4.15A). As a result, the data were not reproducible, and the detection limits were poor (approximately 0.13 $mg \cdot L^{-1}$ Cr^{6+}) (Figure 4.15B).

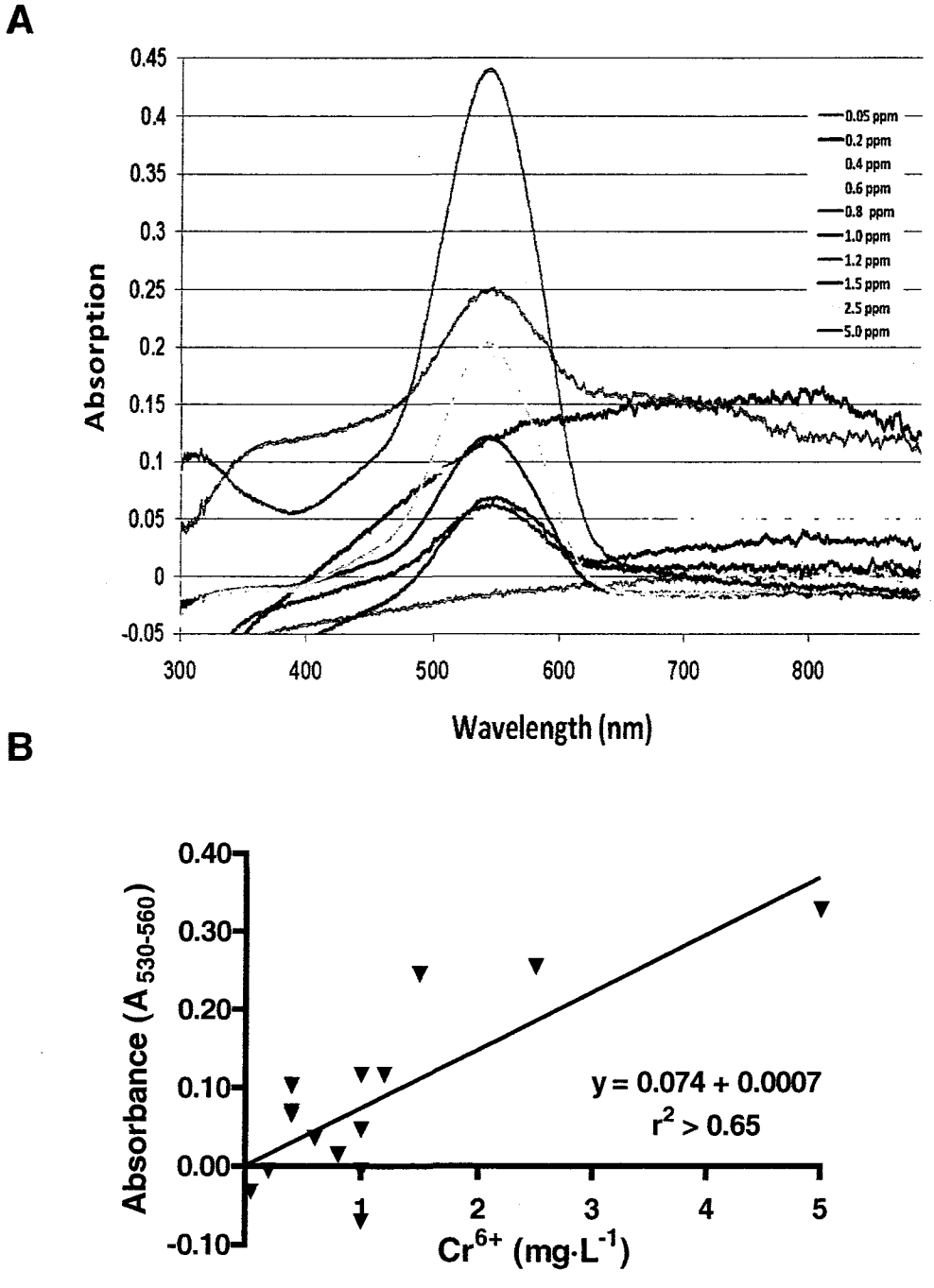

Figure 4.15 Detection of Cr^{6+} using Chromaver3 pellets made in a metal plated pellet press and placed into disc during disc construction. Distorted spectra at lower concentrations (*A*) and resultant calibration curve (*B*)

Apparently a small amount of the chrome metal plating in the pellet press was transferred to the pellets during pressing and affected the lower concentration results. The experiment was repeated using a custom made Teflon pellet press base and parafilm coated plunger. The black deposits on the pellets were eliminated completely and the analytical results were similar to those of standards prepared from unpressed reagents (Figure 4.14 and Figure 4.16).

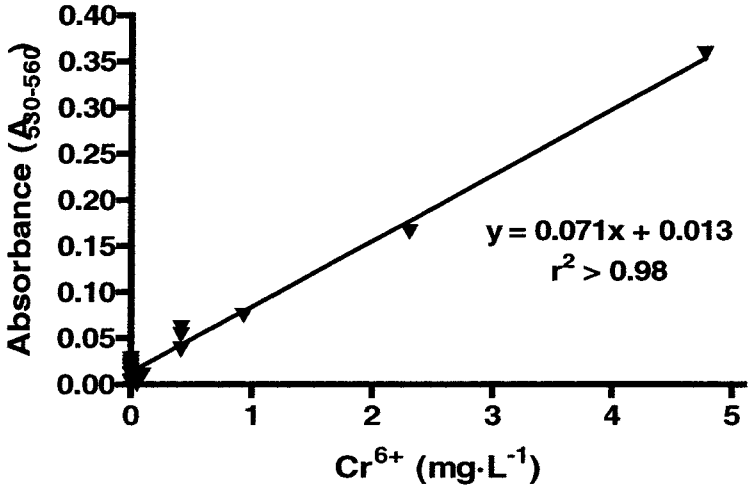

Figure 4.16 Detection of Cr^{6+} using Chromaver3 pellets made in a Teflon/parafilm coated pellet press and placed into disc during disc construction.

The detection limit was 0.03 $mg \cdot L^{-1}$ Cr^{6+} and the linear dynamic range was increased to 5 $mg \cdot L^{-1}$ Cr^{6+}. This detection limit is considered acceptable for industrial point-of-source monitoring. However, the limit of quantification (0.1 $mg \cdot L^{-1}$ Cr^{6+}) is not acceptable for the new EPA/Health Canada regulation of 0.05 $mg \cdot L^{-1}$ hexavalent chromium in drinking water.[82] To meet this requirement, the detection limit would need to be improved by at least a factor of two. The method performs well below this limit with a DL of 0.01 $mg \cdot L^{-1}$ when using the 1 cm cell (Figure 4.17). This suggests that the

problem isn't the chemistry but rather the measurement. Incorporation of a longer path length on the disc would be beneficial and should address this issue.

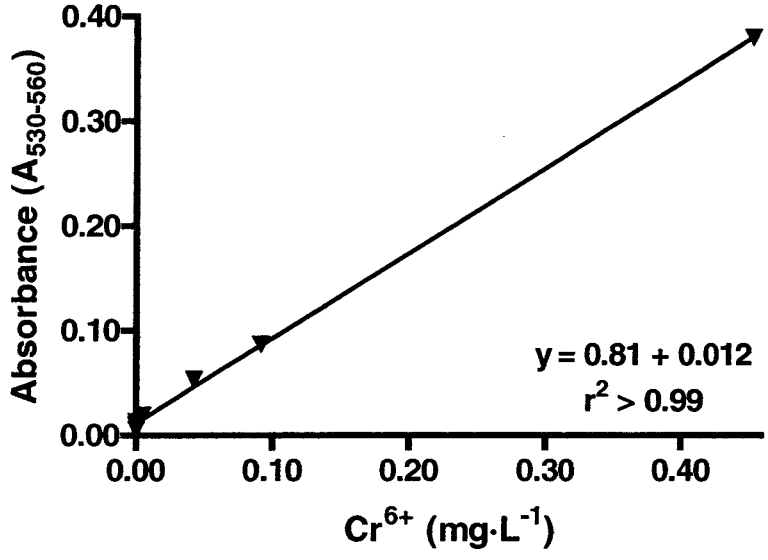

Figure 4.17 Detection of Cr^{6+} at levels below the national drinking water limit using a 1-cm cell and the ocean optics spectrometer, n = 3.

Ideally, this method will be suitable for the detection of hexavalent chromium in real environmental samples. A few spiked wastewater samples were injected onto a pellet containing disc and calibrated using simple aqueous standards. The results were moderately successful with spiked recovery measurements, demonstrating an approximately 130% recovery. The high recovery may be due to the large amount of organic matrix in the samples. Table 4.2 summarizes the results for the Cr^{6+} experiments.

Table 4.3 Summary of calibration parameters for hexavalent chromium (Cr^{6+}) experiments.

Test	Pathlength	Slope	DL	Upper calibration limit
Visual field test	0.5 in	N/A	N/A	1.5 $mg{\cdot}L^{-1}$
Bench top instrument	1 cm	0.7 A / $mg{\cdot}L^{-1}$	0.01 $mg{\cdot}L^{-1}$	1.5 $mg{\cdot}L^{-1}$
Disc (as detection cell only)	1.40 mm	0.08 A / $mg{\cdot}L^{-1}$	0.04 $mg{\cdot}L^{-1}$	5 $mg{\cdot}L^{-1}$
Disc (complete)	1.40 mm	0.07 A / $mg{\cdot}L^{-1}$	0.03 $mg{\cdot}L^{-1}$	5 $mg{\cdot}L^{-1}$

4.4 Conclusions

It is possible to detect nitrite-nitrogen and hexavalent chromium using an *in situ* technique on a centrifugal microfluidic platform. The procedure requires 100 μL of sample or standard, and derivatization and detection can be performed directly on a disc containing dry reagents. In the current disc, 24 individual cells are available and each disc would permit calibration and multiple sample measurements. Both reactions showed molecular extinction coefficients similar to those reported in literature with detection limits of 0.008 $mg{\cdot}L^{-1}$ NO_2^--N and 0.03 $mg{\cdot}L^{-1}$ Cr^{6+}. Reproducibilities of 0.2-3% (n = 3) and 7% (n=3) RSD respectively for mid-range samples, are within the range required for industrial and environmental applications for both analytes. The final on-disc procedure can also be used for detection of both analytes in drinking water as the detection limits are below the maximum permissible drinking water limits (See Chapter 1); however, the limit of quantification for chromium (VI) is above the permissible limit. More importantly, these experiments demonstrated that single step derivatization reactions can

be performed on disc using dried reagents. This opens the door to detecting many other environmentally and industrial important species using pre-prepared discs.

4.5 Future Directions

The typical reaction for detection of nitrate (NO_3^--N) is time consuming and involves multiple steps. A single step nitrate reaction using the Nitraver5 pillow packet was attempted but had poor results. The detection of nitrate was based on the reduction of nitrate to nitrite by cadmium followed by a modified Griess reaction using gentisic acid as the coupling compound. Sensitivity to the length and amount of shaking required and variability in the quantity of the finely divided cadmium during dye formation was thought to be the problem. As an alternative reaction, Jungreis has shown a large scale single tablet method for the detection of nitrate using zinc dust and sulfosalicylic acid followed by diazotization. This method may be amendable for miniaturization.[8] Orthophosphate, sulfate and molybdenum are currently commercially available for large scale analysis in single step reactions and may be possible candidates for miniaturization in further study. Exploration of the experiments outlined above may show further potential for the single step centrifugal microfluidic disc and detection system.

Environmental samples are often much more complex than the simple aqueous standards used in these experiments. Further studies are needed to identify interferences (e.g. organic matter and turbidity) and possible routes to overcoming these interferences. Reagent pellet and disc designs could then be customized to avoid or overcome these issues and provide a more robust analysis method.

There are currently no nitrite or hexavalent chromium certified reference materials readily available.[83] These species are not stable for a long period of time and are often "lost" by conversion into more stable species (NO_3^- or Cr^{3+}). The most common method validation is to spike several samples of varying matrix and demonstrate recovery to be within 75-125%. This would need to be performed prior to using this device on a more widespread scale.

Chapter 5

MIXING, VALVES AND FILTERS

5.1 Introduction

The single cell reactions presented in Chapter 4 are simple one step reactions. In many situations, multiple step reactions or separated sample manipulation processes are required. These may include reactions that require oxidation/reduction, filtration or digestion before derivatization or direct detection. Moving to more complicated multi-step reactions is possible through the use of sequential centrifugal mixing, passive microfluidic valving, and filtering/sedimentation techniques. The advantage of using a microfluidic disc for these multi-step reactions is that all these steps can be controlled by application of centrifugal forces via the rotational frequency of the disc.

Several microfluidic mixing strategies have been previously published.[40,65,84-86] Rotationally induced turbulence is the easiest to implement and works well for mixing liquid samples that do not need to be broken apart.[64]

Multiple valving strategies have been suggested for centrifugal and chip based microfluidic devices.[60-62,65,87] Centrifugal passive valves have the advantage of not requiring active mechanisms but have the disadvantage of allowing vapors through non-physically gated channels. In this chapter, hydrophobic and capillary, valves have been integrated into the polycarbonate discs. Hydrophobic valves pin the fluid by creating an abrupt decrease of channel size in a hydrophobic channel. It is generally accepted that contact angle measurements of greater than 90° suggest the material is hydrophobic.

Capillary valves stop liquid flow at the outside/bottom of the channel due to the capillary pressure barrier created at a sudden expansion in channel size.

The equations in the literature governing passive valve burst frequencies, or the frequency at which the disc must be spun to overcome hydrophobic/capillary forces pinning the fluid to the original cell, are conflicting. The experiments described herein were not meant to verify or test the equations, but instead sought to find a practical valving mechanism that works well within the system as a whole and that can be implemented by using simple manufacturing and assembly techniques. For a more in-depth discussion see the introduction to valves in Chapter 1.

Filtration and sedimentation are often necessary with environmental samples and can consume large amounts of time, require dedicated equipment and can result in analyte loss. Using the techniques presented here, it is possible that filtration and sedimentation can also be integrated directly on the disc to minimize the need for external sample preparation.

5.2 Experimental

All discs were milled in the laboratory as shown in Chapter 2. Experimental discs contained 8 inner 4 mm radius circular chambers, 16 middle 3.86 mm radius chambers, and 8 outer 3.98 mm radius chambers. Eight inner and 8 middle chambers were connected, while the other 8 middle chambers were connected with the outside chambers. The final set of experiments used a disc with 8 inner cells connected by a quartz capillary to 8 middle cells which were connected by a smaller quartz capillary to the 8 outer cells. The disc was rotated using a Parker Automation Servo Motor with Aries Servo Drive (Parker Hannifin Corp., Rohnert Park, CA) and National Instruments Motion Controller.

The motor was controlled by a LabVIEW program (National Instruments, Austin, TX) developed by Ms. Dan (Donna) Peng (McGill University).

For the mixing experiments the discs were agitated for 180 s at 150 RPM with velocity reversal every half turn. The 7-step program is listed in Table 5.1. Depending on the experiment performed, several of the steps may not be needed. For single cell reactions step one and five were used. For the nitrate multi-step reaction steps one through five were used.

Two processes were used to make the connections/valves: channels were cut into the adhesive or quartz capillaries were affixed with clear epoxy into a 1 mm x 1 mm x 5 mm channel milled into the middle layer in the disc assembly. Rectangular channels cut in the adhesive had dimensions of 300μm, 600μm, and 900μm (width) x 5 mm (length) x 100 μm (thickness of adhesive). The channels were used uncoated or modified to be hydrophobic using one of the materials listed in Table 5.2. These dimensions were chosen to provide a maximum difference in burst frequency as estimated from literature and for ease and reproducibility of channel cutting. Quartz capillaries inserted into the disc had 25, 51, 78, or 101 μm inside diameter with a 356 μm outside diameter and were 8 mm in length. The burst frequencies were obtained by increasing the speed in increments of 10 revolutions per minute (RPM) for 20 seconds until at least one full drop of liquid passed through the valve.

Hydrophobic materials were applied by directly applying the material over the bottom and top faces of the discs, but not the sides (adhesive layer) of the channels. If liquids were sprayed onto the disc, a template was used so that only the valve/channel area was coated. For all of the valves, the channel and chamber disc surface areas were

coated with hydrophobic material, the template removed, and the cover sealed on. All materials were sprayed three times with a drying period of 60 min between each coating.

Filtering experiments used three designs to provide on-disc filtration: the "snorkel effect" filter, a hydrophilic polymer filled capillary with 1 μm pore sizes, and a quartz wool plug. The "snorkel effect" consisted of placing the opening of the capillary approximately 1 mm above the bottom of the chamber. This allowed the sedimentation of materials along the outside/bottom of the chamber, below the capillary opening, during rotation. Each filter was testing using 100 μL of: a 400 $mg \cdot L^{-1}$ solution containing 8.44 μm (mean diameter) fluorescence particles (Molecular Probes, Eugene, OR), a 2% solution of 3 μm (mean diameter) Hypersil silica particles (ThermoGroup), or a 5% solution of finely ground soil.

Contact angle measurements were taken using a PAT-1 tensiometer (Sinterface Technologies, Berlin, Germany). The fluorescence microscope images in the filtering experiments were taken using a BX51 research microscope (Olympus America Inc., Center Valley, PA) using a 10x objective lens and an Evolution VF digital camera (Media Cybernetics, Inc., Bethesda, MD). All contact angle measurements and microscope images were taken with the help of Justin Conway and Dr. Rolf Schmidt in the lab of Dr. Christine DeWolf (Concordia University), unless noted. All other photographs were taken using a personal digital camera.

Table 5.1 Mixing program for single step reactions, mixing, filtering, valving and multi-step reaction experiments.

Step	Speed (RPM)	Time	Effect
1	150	180 s	Mixing of first reagent
2	400	180 s	Sedimentation of particles
3	500	150s	Burst valve and fluid transfer to 2nd cell for reaction step 2
4	150	180 s	Mixing of reduced liquid with derivatization agents
5	0	20 min	Reaction time for derivatization reaction
6	750	300s	Burst valve and fluid transfer to 3rd cell for optional reaction step 3

Table 5.2 Contact angle measurements for water on various disc surface modifications.

Material	Manufacturer	Contact Angle θ_c
Uncoated (non-modified) Disc	U-Tech Media Corporation (Taiwan)	77-79°
Super PAP Pen (hydrophobic liquid)	Daido Sangyo Co. Ltd. (Greenwich, CT)	87-89°
Teflon Tape	N/A	120° (see 88)
Elite Professional Grade Protector (hydrophobic spray)	Icon Industries, Inc (Montreal, QC)	106°
Fused Silica Capillaries	Polymicro Technologies (Phoenix, AZ)	33° (see 89)

5.3 Results and Discussion

5.3.1 Mixing

Efficacious mixing in microfluidic devices can be difficult due to the laminar flow caused by the small dimensions encountered in these devices. In these experiments "shake-mode" or "batch mode" mixing was used as a simple, rapid approach to mix the dry and wet reagents.[64] When a disc rotates the Coriolis pseudo-force puts pressure on the liquid to move outward in a straight line perpendicular to the direction of rotation. The continuous changes in disc velocity induces a twisting/swirling pattern caused by liquid colliding with the walls of the chamber as the disc changes direction.[65,67] The advective currents produced increase the surface area between the mixing components causing faster mixing. The mixing schemes used in the experiments are listed in Table 5.1. Two liquids were completely mixed in less than 9 seconds as shown in Figure 5.1. All solid reagents used in these experiments were highly soluble and dissolved quickly but a total mixing time of 180 seconds was used due to manufacturer's recommendation for mixing the reagents by hand. The mixing time is sufficient for complete mixing as shown by the lack of visible solid granules and the consistent results in this chapter and in Chapter 4.

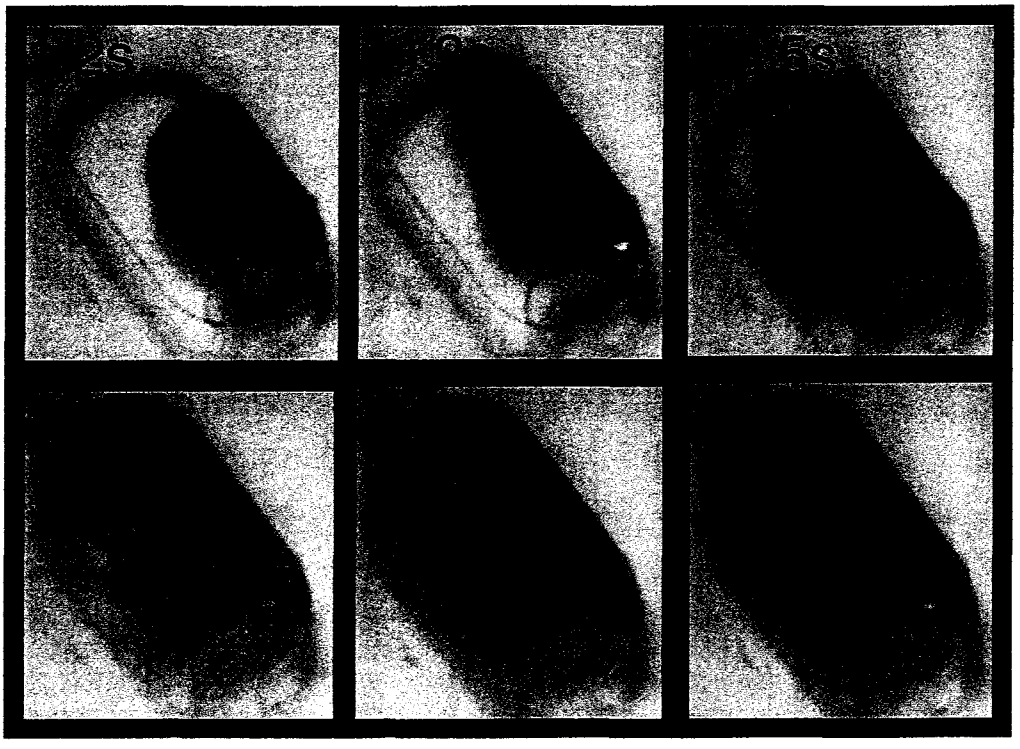

Figure 5.1 Photographs of 10 μL red dye mixing in 100μL of water at 150RPM with a velocity change every ½ rotation of the motor.

5.3.2 Valves

To provide the ability for multiple step reactions, several types of valves were constructed and investigated. Both categories of valves, hydrophobic and capillary, are governed mainly by the surface tension of the liquid, the contact angle (θ_c), the diameter of the constriction, and the mean radial distance of the valve.[63] The surface tension (γ) of the liquid in these experiments was kept constant by using dyed water ($\gamma = 10^{-1}$ N m^{-1}) for all the experiments.[63] The contact angle of water on the various materials used to make the valves is listed in Table 5.2. For each substrate (hydrophobic or hydrophilic) the contact angle of the liquid on that substrate would be same. Hence, only the diameter of the constriction was varied for each substrate, but the contact angle varied between substrates.

To provide sequential valving the contents of the first cell (inner cell in most centrifugal apparati) must be allowed to move to the second and then to the third cell only when the user desires. The easiest strategy to accomplish this is to make the first valve with a lower burst frequency than the second (outside) valve (Chapter 1, Equations 1-4).[66] This is accomplished by employing larger diameter valves (constrictions or expansions) from the inner to the middle cell and smaller diameter valves (that require higher burst frequencies) from the middle to the outer cell.

The simplest way to implement a valve on laminated microfluidic discs constructed in the laboratory is to cut a channel from an inner cell to an outer cell in the adhesive layer used to seal the discs together. The discs are made of polycarbonate which has a contact angle of about 78°, making it slightly hydrophilic. Polycarbonate is considered in industry to be neither hydrophobic nor hydrophilic. Approximately 75% of the valve channels, made on discs with no surface treatment, filled with a dye solution by capillary action immediately after it was injected onto the disc (Figure 5.2). The capillary barrier pressure at the meniscus prevented leakage into the outer (next) cell. In the remaining 25% of the devices, the valve channel did not fill until the disc was spun at a low speed causing the pressure on the liquid to increase, resulting in the liquid being pushed to the outside/bottom of the channel. The valves constructed with no surface treatments were very sensitive to any variation in the surface properties caused by contaminants such as dirt or fingerprints.

The outside valve (at an average radial position of 4.4 cm) consistently had lower burst frequencies than the inside cells (at an average radial position of 3.2 cm) due to the increased centrifugal force applied to the barrier pressure at the sudden expansion, as

expected from theory (Chapter 1, Equations 1-4).[62,63] The smallest outside valve (300 μm) burst at an average of 230 RPM, while the largest inside valve (900 μm) burst at an average of 320 RPM (Figure 5.3). The large standard deviation in the burst frequency would not allow controlled, sequential valving on a disc. This and the inverse in burst frequency/size trend suggested that further use of an uncoated valve is impractical.

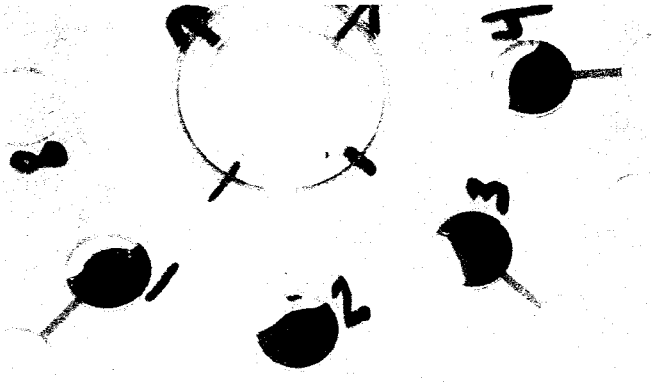

Figure 5.2 Channels made in 100 μm thick adhesive on uncoated polycarbonate. (Shown 30 s after injection of 100 μL of red dye) Note that channels 1, 3 and 4 have wetted but channel 2 has not.

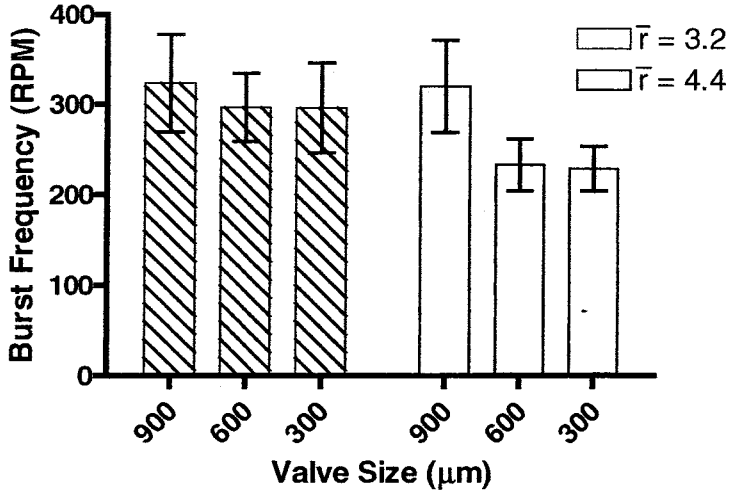

Figure 5.3 Burst frequency of valves created using adhesive channels on polycarbonate. Error bars are one standard deviation (n =8).

According to theory, increasing the contact angle, by changing the hydrophobicity of the valve substrate, will increase the separation in the burst frequencies of the inner and outer valves.[61-63] Several surface modifications were made to the disc to increase the contact angle (Table 5.2). A liquid hydrophobic polymer used in immunohistochemistry was applied to the discs that formed the upper and lower walls of the valve channel. Unfortunately, this liquid polymer was too viscous and caused blockage of the channel. Placing a thin layer of Teflon tape across the upper and bottom channel was also attempted but caused leakage throughout the disc because of the lack of adhesion of the Teflon to the adhesive layer. A hydrophobic polymer spray used in the clothing and shoe industry was used to create a hydrophobic surface on all sides of the valve and increased the contact angle to the intermediate value of 106°. In this case the device sealed correctly and the burst frequency experiment was repeated, the results are shown in Figure 5.4.

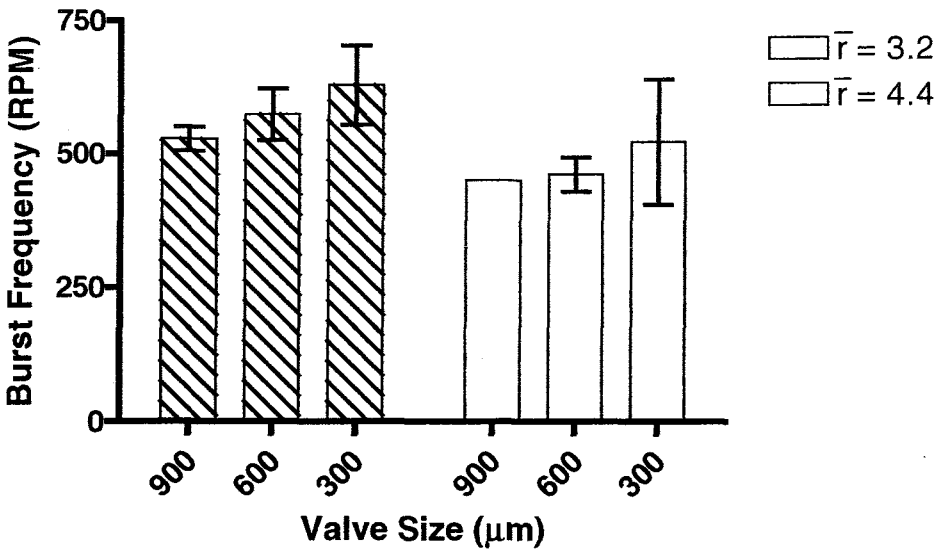

Figure 5.4 Burst frequency of valves created using adhesive channels on a polycarbonate surface modified with a hydrophobic spray. Error bars are one standard deviation (n = 8).

As expected, the liquid remained at the restriction between the cell and channel top and the burst frequencies for both valve positions increased.[60,61,63] The burst

frequencies trended as expected with the wider valves having lower frequencies. The smaller relative standard deviations may be from the more uniform disc surface after the spray coating. The increased centrifugal force due to the larger radial position of the outside valve caused a lower burst frequency. Unfortunately, in both adhesive valve studies there wasn't any combination of valve size (hence burst frequencies) that would allow for sequential valving.

In order to compensate for the increase centrifugal force at the outside position, smaller valve sizes were needed. To overcome the lack of resolution and reproducibility of the xurographic cutter, quartz capillaries were used as valves. This involved an extra construction step (described in Chapter 2), but avoided the need to modify surface properties or use time consuming techniques, mentioned in Chapter 2 (lithography, micromachining, bonding), traditionally used to obtain microchannels. Again keeping the same disc design with cells at 3.2 and 4.4 cm, the experiment was repeated.

The 51-μm and 78-μm diameter capillary valves at the outside position had a significantly higher (p = 0.0001, by t-test) burst frequency than the 101-μm diameter inside valve. Of the eight, 25-μm valves tested, all except one 25-μm outside valve did not burst at the maximum motor speed of 2500 RPM. This failure could have been due to a sealing of the capillary when the epoxy was applied or an inaccurate capillary cut could have crushed the quartz and clogged the column. The value provided in the graph below is for information only and needs to be confirmed with further testing.

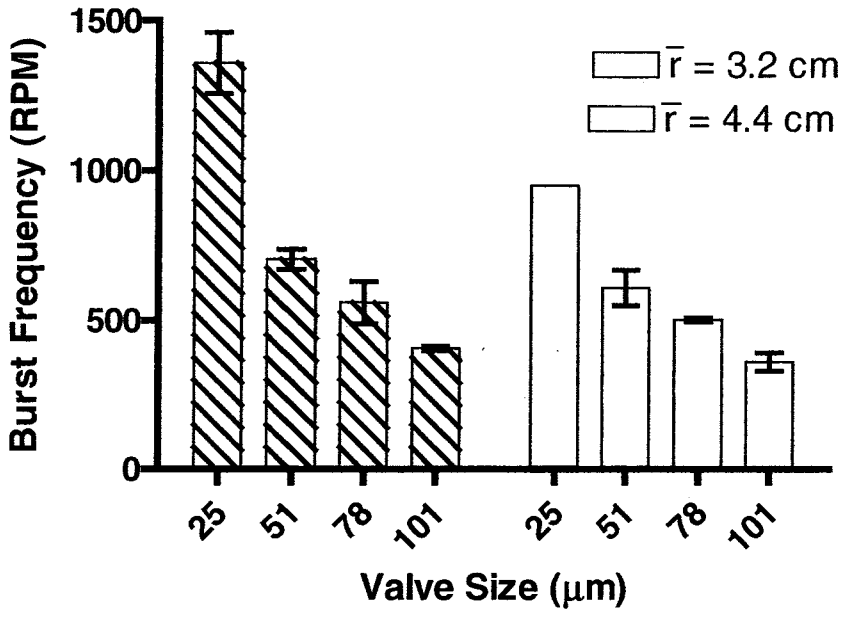

Figure 5.5 Burst frequency of valves created using quartz capillaries. Error bars are standard deviation (n = 8). For the 25-μm, 4.4-cm valve (shaded) n = 1, value provided for information only.

In the case of the capillary valves, the relatinship between capillary diameter and the force required to overcome the meniscus force is well behaved and follows the theory presented in Chapter 1. The liquid was held, or pinned, to the outer wall of the inside chamber until the centripetal force exceeded the capillary barrier pressure. To test sequential valving a disc with 101-μm and 51-μm capillaries as the inside and outside valves was constructed. The test liquid stayed in the inner chamber (see Figure 5.6, 0 s) until the rotational speed (500 RPM) exceeded the burst speed of approximately 400 RPM (Figure 5.5). The pressure induced by the centrifugal force caused the normally concave meniscus formed in the hydrophilic capillary to invert, allowing the valve to "burst" and to begin to form a drop (Figure 5.6, 1.6 - 6.4 s).[63] After the drop formed (Figure 5.6, 6.4 s), the remaining liquid flowed quickly and smoothly through the wetted valve into the second chamber (Figure 5.6, 15 - 18.4 s). A tiny amount of fluid was drawn

into the second quartz valve by capillary action, but did not burst (Figure 5.6, 120.7 s) until the rotational frequency was increased above its burst speed. When the disc speed was increased to 750 RPM, more than enough force was provided to overcome the higher surface tension present at the exit of the smallest capillary and the second valve burst allowing fluid transfer to the outside chamber.

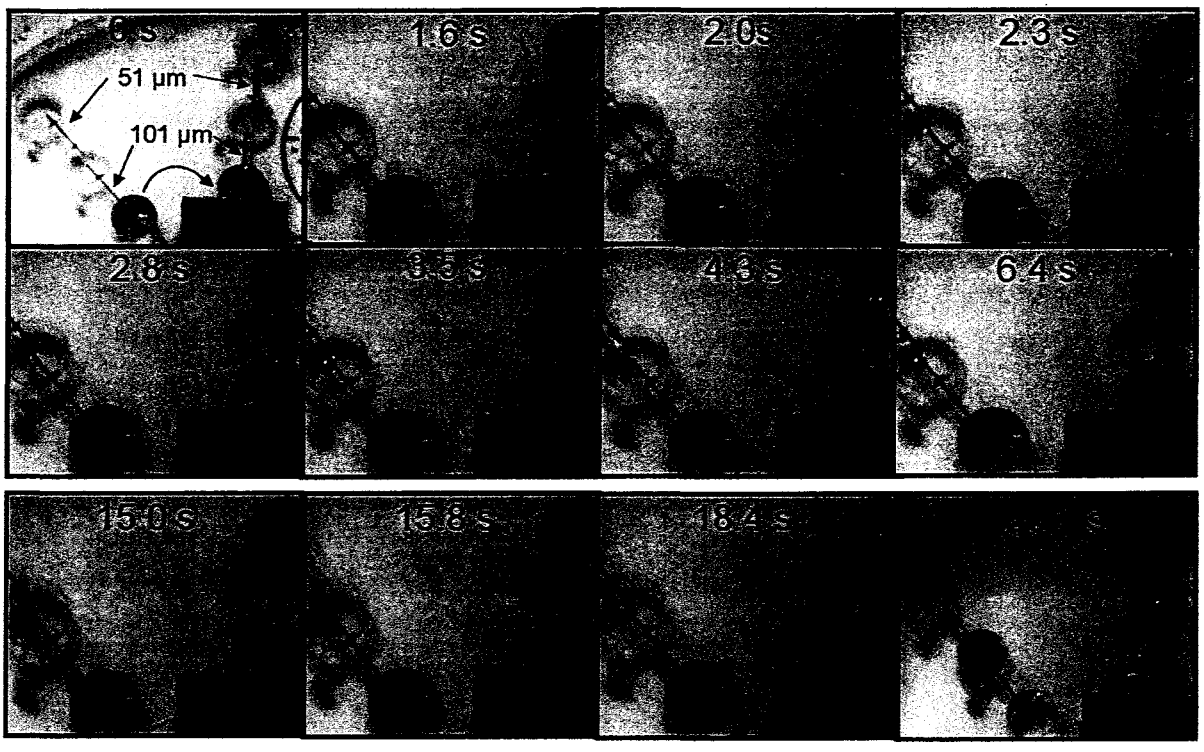

Figure 5.6 Strobe photographs of capillary valving using quartz capillaries inserted onto the disc during construction. The disc was spun in the clockwise direction at 500 RPM for a total of 120.7 s. Top section shows wetting, burst and initial droplet (< 6.4 sec). Bottom section shows faster flow after initial valve wetting (~ 3.5 sec per drop).

5.3.3 Filtering

Many samples contain particulate matter and require some form of filtering before analysis. In particular, environmental samples may need filtering after initial mixing to prevent solid precipitates and potential sediments from interfering with a second reaction

step. Three types of filters were investigated: a sedimentation, or "snorkel effect" filter, a porous polymer physical filter and quartz wool physical filter.

The sedimentation filter is conceptually the easiest as it is just a capillary burst valve with the inlet extended well into the inner/upper liquid chamber. This arrangement required only minimal alteration in disc design. The quartz capillary inlet was placed about 1.5 mm above the bottom of the cell, allowing room for particles to sediment beneath the valve inlet (Figure 5.7). The particles were sedimented by slowly ramping the speed to just below the burst frequency and then holding for 30 s. Once the particulates were sedimented, the valve was burst by increasing the rotational speed. This strategy worked well for the 3-μm silica particles, the ground soil sample (Figure 5.7), and the 8 μm fluorescent particles (Figure 5.8). In Figure 5.7A, the upper cell is filled with the silica suspension. After sedimentation, the liquid in the lower chamber visually appeared clear of the white silica particles (Figure 5.7B). This was the case for sedimentation of the finely ground soil also (Figure 5.7C).

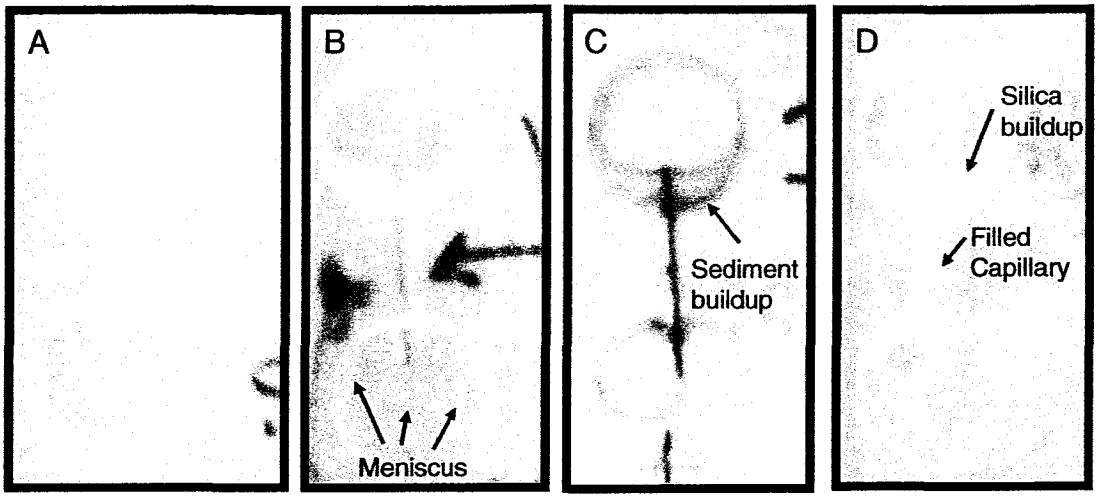

Figure 5.7 Photographs of filtering experiments. 3-μm silica in suspension before sedimentation (***A***). Sedimentation of 3-μm silica using the "snorkel effect" filter (***B***). Finely ground soil sediments below "snorkel" after spinning (***C***). Silica buildup, initial solution seen in (**A**), in top cell using a polymer filled capillary as a filter (***D***). Dimensions listed in section 5.2.

A microscopic image of the initial solution of 8-μm fluorescent particles is seen in Figure 5.8A. The solution, after filtration by "snorkel effect" sedimentation shows approximately 4 times less particles for the same magnification (Figure 5.8C).

Figure 5.8 Fluorescent images of 8 μm particles in initial solution (***A***) after filtration with filled capillary (***B***) or by sedimentation using the "snorkel effect"(***C***). All images used the same magnification.

The second filter tested used a porous polymer filled capillary as both a burst valve and physical filter. The capillaries were prepared by Mr. Wei Lin and Dr. Jean-Louis Cabral (Concordia University) following the protocol developed by Bandilla et *al.*[90] The 75 μm inner diameter capillaries were filled with a porous polymer monolith

that has an approximate 1 μm pore size. A small amount, compared to none seen in the "snorkel" filter, of soil and 3-μm silica were seen in the porous polymer filter although it is not noticeable in Figure 5.7D. However, the porous polymer filter worked better than the sedimentation technique for the 8 μm diameter fluorescence beads. The microscope image showed half the number of particles in the solution after filtering through the filled capillary than seen after filter by the snorkel effect (Figures 5.8B and 5.8C).

These data suggest that there may be a density effect. Silica and soil are high density materials and sediment easily and rapidly but the latex beads sediment slowly and may still have been suspended when the "snorkel" sedimentation filter broke. On the other hand the filled capillary physical filter would be a size based filtration and would be expected to do better on the 8 μm particles than the 3μm silica. However, if a hydrophobic porous polymer were available (to increase the burst frequency of the filled capillary), a combination of the "snorkel effect" and the physical polymer filter would be superior and should prevent all the particles from passing. The third filter type, a quartz wool plug, failed all tests and no further experiments were performed using that type of filter. The failure was most likely caused by an inefficient plug packing technique. Quartz wool plugs have been used to prevent 5 μm solid phase extraction chromatography particles from leaving a 100μm column incorporated on a disc by colleagues in the same laboratory.

5.4 Conclusions

Consistently using "shake mode" mixing provides a more reproducibly mixed sample than shaking by hand and eliminates the cost and complexity of miniaturized

elements added onto the disc to create turbulence as seen in other microfluidic designs (*e.g.* beads). A simple and predictable quartz capillary based valving mechanism that does not involve complex design or fabrication processes has been implemented on a microfluidic disc. The use of pre-made quartz capillaries avoids the need for surface modification and allows the use of multiple material types for disc fabrication. Efficient filtration of up to 75% of particles, which is adequate for many applications, from 8 μm to 3 μm in size has been accomplished using either physical filtration or sedimentation. Given the simplicity of preparing the sedimentation filter, this was the design used for the nitrate reactions reported in Chapter 6. When the sedimentation filter was used with cadmium particles from the nitrate reduction, no particles were visually seen in the second cell. More importantly, the possibility of using multiple valves for 3-4 step reactions has been demonstrated.

5.5 Future Directions

Due to contradictory explanations in the literature of the equations governing the flow of liquids by a change in valve geometry, further studies are necessary to establish an adequate theoretical framework for the quartz capillary valve findings. The influence of the beta angle (β), the angle at which the chamber walls fall away from the restrictive channel, the aspect ratio, the ratio of depth to width of the channel, length of the channel, and the surface properties of the channel and chamber (*i.e.* hydrophobic or hydrophilic) need further study to help predict a more precise burst frequency.

Although not elaborated upon here, the packed capillary used as a valve and filter is in fact used for chromatographic separations and could easily be used to include chromatographic separations directly on the disc. Frontal chromatography would be the

easiest to implement.[91] Control of flow rate of liquid through the column and detection would need to be further studied.

In addition to sequential valving, flow splitting is possible by placing two capillaries in an inverted V-shape (because the top and bottom are at the same radial distances) and should cause the liquid to split into two cells but the Coriolus effect may ultimately cause the liquid to flow into a single channel as the liquid is drained.

The most notable future direction for a complete analysis on disc would be the filtration of samples through a 0.45 μm pore diameter filter, which is the standard used for analysis of natural waters. This could be accomplished with a combined or modified sedimentation/filled capillary technique or a separate shaped frit place directly on the disc before the burst valve.

Chapter 6

MULTI-STEP REACTIONS ON DISC: NITRATE (NO_3^-)

6.1 Introduction

The number of single step reactions readily available for incorporation into portable microfluidics discs is limited due the availability of stable dry reagents and the complexity of reactions needed for derivatization of analyte species. By using the valves and filters presented in Chapter 5, multiple step reactions are possible and open the door to a vastly larger number of reactions (and sample manipulation steps) that can be performed on a microfluidic disc. It was demonstrated in Chapter 4 that nitrite (NO_2^-) can be derivatized and detected directly on a microfluidic disc in a single step. Nitrate (NO_3^-) can also be detected by initially reducing the nitrate ion to nitrite using cadmium metal (Cd^0) as a reduction catalyst (Figure 6.1) followed by detection of the nascent nitrite (NO_2^-) using the modified Griess reaction shown in Chapter 4.

$$NO_3^- + 2H^+ + Cd^0 \rightarrow NO_2^- + H_2O + Cd^{2+}$$

Figure 6.1 Redox reaction for the reduction of nitrate to nitrite using cadmium.

After multiple trials runs for the detection of nitrate using a chemistry that involved the reduction and derivatization of nitrate in a single step, it was determined that the precision, accuracy and dynamic range continued to be unacceptably poor. This was thought to be due to interferences caused by the presence of cadmium during the derivatization and detection steps. Thus, a two step reaction should improve detection of nitrate (NO_3^-) by first reducing it to nitrite (NO_2^-) using cadmium metal (Cd^0) in the first

reaction cell and then transferring the nitrite solution to a second cell for derivatization and detection. This strategy requires that the initial nitrite concentration is known (or measured using the single step reaction shown in Chapter 4) so that the nitrate concentration can then be found by difference.

It is known that calcium (Ca^{2+}) and chloride (Cl^-) concentrations over 100 $mg \cdot L^{-1}$ interfere with nitrate detection. A high chloride concentration, such as seawater, will cause low results but can be overcome by standard additions. On the other hand, ferric ion (Fe^{3+}) and nitrite (NO_2^-) ion interfere at all levels. Additionally, samples at extreme pH, or which are highly buffered, may exceed the capacity of the packaged buffering agents and require an off-disc pretreatment step.[92] The large scale experiments that have been miniaturized in the following experiments show a reaction sequence that takes two steps to implement. More steps could be implemented with additional valves, filters and/or separation steps.

6.2 Experimental

The contents of Nitraver6 and Nitriver3 obtained from Hach Company (Loveland, Co) are listed in Table 6.1 and are the required reagents for the two step nitrate detection reaction. All water used to make standards was distilled and deionized. All standards were made with 1000 $mg \cdot L^{-1}$ nitrate calculated as nitrogen (NO_3^--N) from SPEX CertiPrep®, Inc. (Metuchen, NJ). Pérade-20 was obtained from Environment Canada National Water Research Institute (Burlington, ON) and is certified as 0.228 ±0.003 $mg \cdot L^{-1}$ NO_3^--N and NO_2^--N (95% CL).

Table 6.1 Contents of Nitraver6 and Nitriver3 packets.

Nitraver6®	Nitriver3®
Potassium Pyrosulfate	Potassium Pyrosulfate
Potassium Phosphate, Monobasic	Potassium Phosphate, Monobasic
1,2-Cyclohexanediaminetetraacetic Acid Trisodium Salt	1,2-Cyclohexanediaminetetraacetic Acid Trisodium Salt
Cadmium	Chromatropic Acid, Disodium Salt
Sodium Sulfate	Sodium Sulfanilate
Magnesium Sulfate	

For the large scale experiments, a single Nitraver6 packet was added to a clean vial along with 10 ml of standard or sample. The suggested reaction time (accompanied by shaking) was 3 minutes. Any un-oxidized metal was allowed to settle during a 1 minute period after which 5 ml of the solution was moved to a clean vial. A single packet of Nitriver3 was added and the vial was agitated for 30 seconds. After a 20 minute reaction period the absorbance was measured using a bench top spectrometer.

A disc was constructed with one 5 mm radius chamber at an average radial distance of 32 mm. The chamber was loaded with approximately 8.7 mg (6.9-10.4 mg) of pelleted Nitraver6 and was connected by a 78 μm quartz capillary to a second 4 mm radius chamber containing approximately 5.3 mg (4.0-6.7 mg) of pelleted Nitriver3 (Figure 6.2). After injection of 100μl of a known standard solution, the experiment followed the mixing protocol listed in Table 5.1. All absorbance results were calculated using the ratio method described in Chapters 3 and 4 for the determination of nitrite-nitrogen (NO_2^--N).

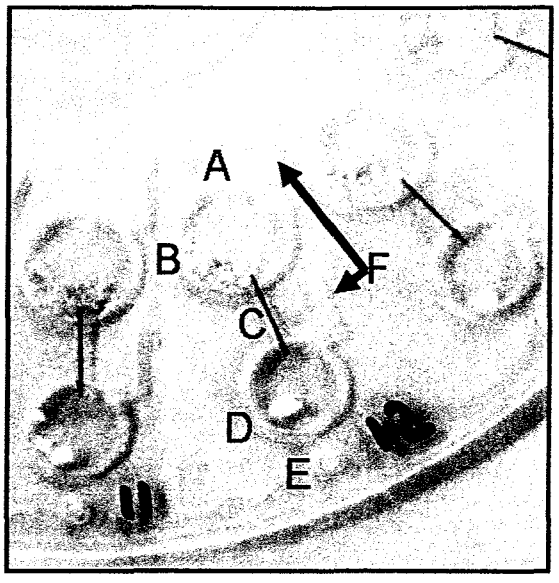

A. Sample Injection port

B. Nitrate Reduction Reagents (r = 5 mm)

C. Quartz Capillary Column/Filter

D. Nitrite Derivatization Reagents (r = 4 mm)

E. Detection Alignment Hole

F. Vents

Figure 6.2 Centrifugal microfluidic disc for the reduction of nitrate to nitrite using cadmium and detection via derivatization.

6.3 Results and Discussion

The detection of nitrate is notoriously difficult due to the number of factors that influence the reduction rate and efficiency and the subsequent formation of the azo dye in imperfect conditions.[33] Consequently, reduction methodologies vary throughout academic and industrial literature. The Hach Nitraver6 method was chosen for its ease of use and adaptability. The nitrate ion is almost quantitatively reduced to nitrite by cadmium in the range of 0.01-1 $mg \cdot L^{-1}$ NO_3^--N and is the recommended procedure for nitrate concentrations less than 0.1 $mg \cdot L^{-1}$ due to lack of sensitivity in other methods.[20]

The large volume (10 mL) experiment was performed to verify the procedure and acquire results for comparison. The spectra were similar to the results for nitrite (NO_2^-) as expected with no spectroscopic anomalies (note: the spectra in Figure 4.7 have a 1.4 mm pathlength), suggesting there were no interfering species from the added reduction step (Figure 6.3). The calibration curve was linear with a respectable linearity ($r^2 > 0.98$). The

reproducibility was variable (2-20%), with the highest deviation at the upper and lower ends of the range (Figure 6.4).

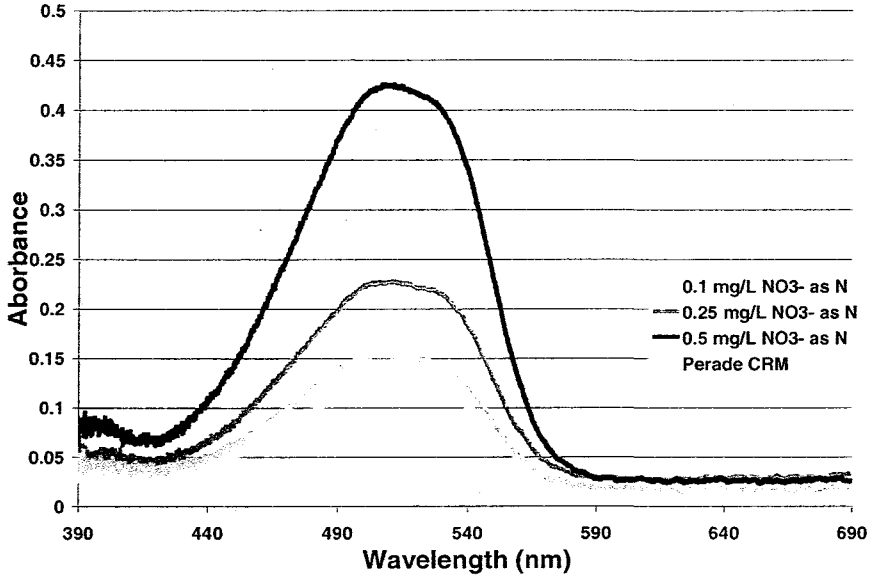

Figure 6.3 Absorbance spectra after reduction from nitrate (NO_3^-) to nitrite (NO_2^-) and derivatization in large volume experiments (1 cm path length).

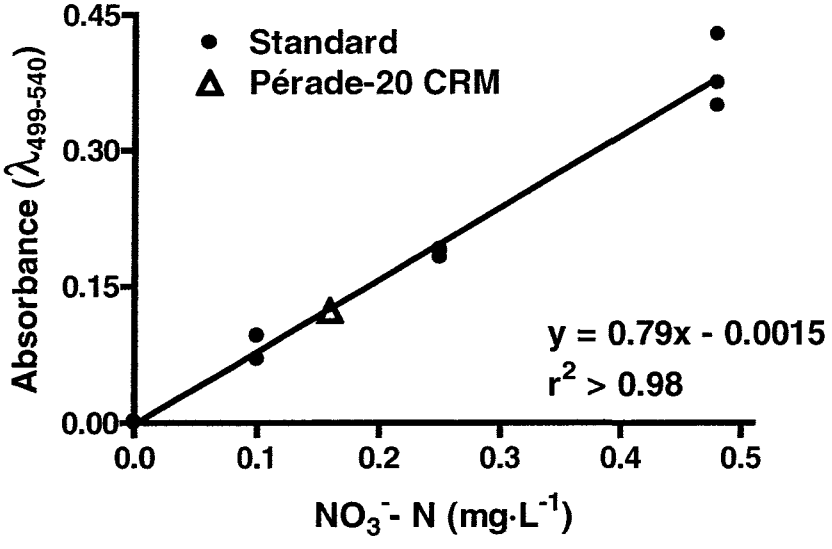

Figure 6.4 Large volume experiment calibration data for nitrate nitrogen (NO_3^--N) using a 1 cm cell. The Pérade-20 reference material is certified to 0.228 $mg \cdot L^{-1}$ NO_3^- -N (n = 3).

There was low recovery of the standard reference material in the large scale experiments at 0.15 $mg \cdot L^{-1}$ instead of 0.228 $mg \cdot L^{-1}$. Pérade-20 is derived from soft river water and should contain no known interferences. A series of standard additions could have been performed on the reference material to validate the results above. This would have shown if there was any matrix effect from the reference material or if the reference material had been contaminated. In the interest of time those experiments were not performed.

Interestingly, the nitrate (NO_3^--N) curve, which is detected as nitrite (NO_2^- -N) after reduction, has a sensitivity of 0.79 $AU/mg \cdot L^{-1}$, less than half that of the nitrite (NO_2^- -N) standard curve found in Chapter 4 of 2.0 $AU/mg \cdot L^{-1}$. This difference in slope has been noted in the literature, with little explanation, when using zinc (Zn^0) as the reduction metal, but not specifically when using cadmium (Cd^0).[36,37]

The cadmium reduction method used in this experiment has been noted to be extremely dependent on the type of cadmium used, the amount of dissolved oxygen, the chloride (Cl^-) content, the pH, and the particle size. This has been demonstrated to be true for techniques using shaking and packed reduction columns.[6,26,33-35] Even with the aforementioned difficulties, the EPA/Environment Canada suggested method for detection of nitrate (NO_3^--N) is via reduction using a cadmium (Cd^0) column providing a large surface area to ensure contact of the molecules for a complete reduction.[20]

Although reduction with either pure cadmium, copperized cadmium or zinc columns have been reported with relative standard deviations of 0.91% to 2.9% when performed by a single laboratory with relatively ideal samples[6], after discussion with industry representatives[93] a reproducibility of 9-20% and a recovery of around 75% was

deemed realistic using these reagents and is generally acceptable. The efficacies of future experiments were based on these numbers along with comparison to the large volume calibration.

The large volume experiment was reproduced using the disc as a detection cell only. The results were similar to those of the large scale experiment with the expected slope of 0.11 AU/mg·L^{-1} due to a reduction in path length (Figure 6.5). A reproducibly of 14-16% RSD and a recovery of 67% for the Pérade-20 certified reference material was within the expected range. There was little to no error introduced to the system by using the disc as a detection cell. The detection limit was 0.04 mg·L^{-1}, close to the expected limit, as compared to DL of 0.006 mg·L^{-1} from the large volume experiment.

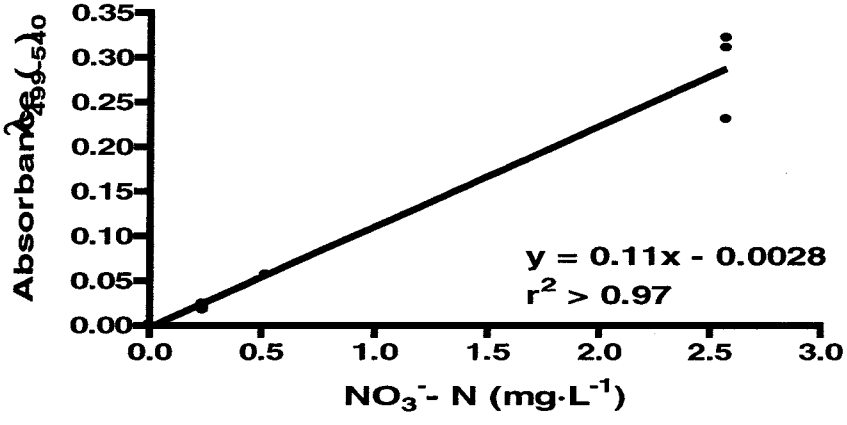

Figure 6.5 Detection of NO_3^--N in a 1400 μm disc cell after separate reduction and derivatization outside of the disc (n = 3).

To determine if each step of the reaction could be carried-out on the disc while avoiding the potential complications of material not being adequately filtered a disc was constructed without any capillary valve/filter channels. This disc was loaded with the

appropriate amounts of reagent in the inner and outer cells and sample introduced into the first (inner) cell. Mixing, reaction and finally sedimentation of any unoxidized metal was carried out before the reduced solution was manually pipetted to the outer cell containing the second reagent. This method showed results with a correlation coefficient of $r^2 > 0.98$ and repeatability of 25% RSD (Figure 6.6). The slope was equivalent to the calibration when the reactions were done outside of the disc. These results demonstrate that micro-quantities of reagent in pellet form will work for the linear detection of nitrate (NO_3^--N) on a microfluidic disc. The background absorbance ratio calculation method (Chapter 3) increased the precision of the measurements but cannot overcome interferences from light scattering due to bubbles in the cell. Several data points were excluded due to bubbles that formed in the detection/reaction cell and caused grossly negative or positive absorbances as determined by a *Q*-test.

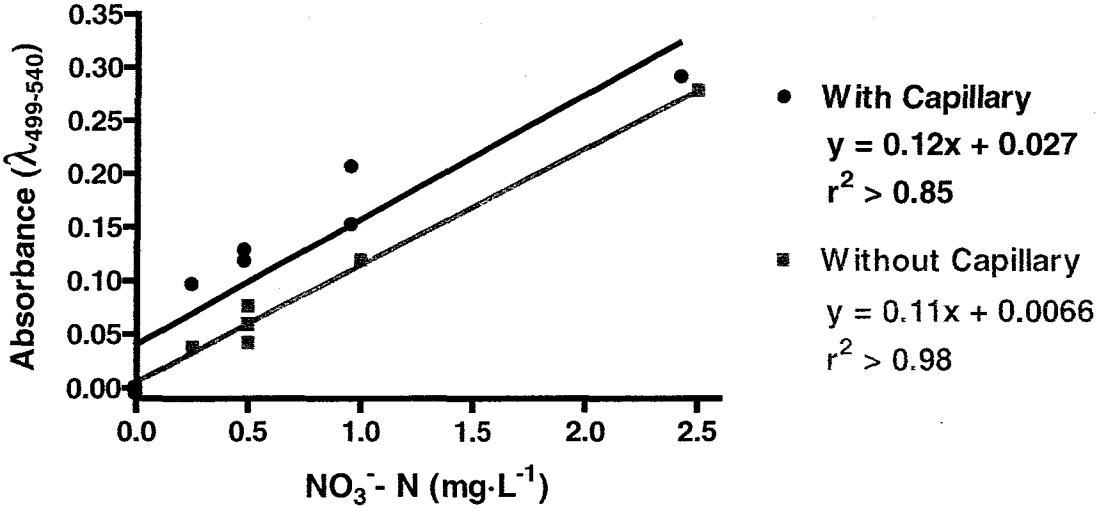

Figure 6.6 Calibration curves for NO_3^--N with reduction and derivatization on a microfluidic disc using dry reagent pellets. Top curve incorporates capillary valving bottom curve is manually transferred.

The experiment was repeated incorporating the capillary valve/filters. The slope (0.12 AU/mg·L^{-1}) was similar to the expected slope but showed a non-zero y-intercept (0.02 AU), even though multiple zero points are included in the data set (Figure 6.6). The slope displayed a linear correlation of $r^2 = 0.85$ and the detection limit was 0.57 mg·L^{-1}. The increased number of cells with bubbles adversely affected the reproducibility and degraded the detection limit.

As seen in Figure 6.6 most of the non-zero data points were above the trend line. If the zero points are excluded from the capillary data set the equation of the line changes to Absorbance = 0.088[NO_3^- (mg/L)] + 0.096 with a correlation coefficient of $r^2 = 0.93$. The non-zero intercept is due to an apparent deviation in Beer's law caused by either an improper blank measurement or different conditions between the blank and standard measurements. Non-analyte species could be absorbing in the standards causing the positive intercept or a change in the refractive index of the standard solution compared to the blank could be causing reflection losses.[75] Contamination was most likely caused by the epoxy or spectral interference from other absorbing species generated by Cd or its by-products. Human salt (on the skin) which could have been introduced during disc construction may also have had a low level of nitrate/nitrite in it causing the positive deviations. Simple control experiments could rule both epoxy and salt out. Visibly, there were no cadmium particles in the detection cell, but the work with filtration in Chapter 5 showed that particles can be transferred even though they were not visible. Improper disc ventilation and/or any dissolved cadmium may have adversely affected the diazotization in the second cell.

Complicating the issue further, the 2nd reaction cell on the disc was designed for 100 μL of solution that was added to the upper cell but approximately 10-20 μL of the reduced solution was retained in the upper cell after the valve burst, due to disc design and sedimentation (Figure 5.6, 120.7 s). The bubbles could have been caused/increased by the excess reagents in the second regent pellet as the mass was not adjusted for the smaller volume. A change in disc design may improve results or show that it does not effect the reaction.

Jones *et al.* demonstrated that spongy cadmium was more effective in nitrate reduction than cadmium granules (such as those used in this method) and that erratic results were found if too little cadmium was used, but not when used in excess.[34] The Nitraver6 pellet loaded on the disc contained 6-10 times the amount of material suggested by the scaled-down manufacturer's procedure. This was to insure that both the amount of cadmium and the buffer reagents were in excess and to accommodate the pellet making process as production of pellets any smaller rendered them too difficult to handle. The capillary disc showed higher absorbances on all the standards used, which was unexpected, as the blanks and general spectral shape for both with and without the capillary were similar. If too much cadmium was used, it is possible that the nitrate (NO_3^-) was further reduced in some of the cells and was not detected by the diazotization reaction, however this would cause low results, not higher.

It is known that agitation time and technique have a large influence on reduction efficiency.[34, 92] The agitation time for both discs was 3 minutes. All cells were at the same radial position and should have been agitated in a very consistent manner. Theoretically, the disc method should be more precise than agitating by hand or by agitating

mechanically, which was utilized in the large volume method. Too short an agitation time can cause erratic results due to incomplete conversion of nitrate to nitrite. Conversely, agitating too long can reduce dissolved oxygen, overcoming the buffering capacity, and changing the pH for the diazotization reaction. This is unlikely as the disc provides an almost completely sealed system. Dissolution of cadmium by dissolved oxygen has been shown to be the dominant reaction for large scale reductions.[33] These reactions were performed at an acidic pH of 4. In all cases reported in the literature, the reactions performed at a basic pH had more accurate and precise results.

6.4 Conclusions

In this chapter a microfluidic disc with multi step reaction chemistries was demonstrated and is a significant step towards a fully integrated microfluidic platform for a wide variety of analyses. All reagents needed for the reduction of nitrate (NO_3^-) to nitrite (NO_2^-) and the subsequent diazotization of nitrite were incorporated onto the microfluidic disc in two stable reagent pellets separated by a burst valve. Imprecision and possible contamination were caused by chemistries that are not well understood but are most likely not due to the fundamentals of disc design as similar problems were seen at all reaction scales and throughout the literature. Even so, the method can detect samples below the recommend drinking water standard for nitrate of 10 $mg \cdot L^{-1}$ NO_3^--N.

6.5 Future Directions

Ideally, a cadmium column or frit could be introduced onto the disc mimicking the micro-flow injection analysis systems such as that shown by Petsul *et al.* and

Jannasch *et al.*[31,49] Establishing the flow rate through the frit would need to be studied before incorporation into a microfluidic device. Copperized cadmium, as opposed to the pure cadmium used in the Nitraver6 reagent, has been show to give more precise results. The effect of the cadmium being used up from reducing diatomic oxygen instead of nitrate, as well as, the effect of dissolved oxygen causing a shift in pH due to the formation of OH^- and/or consumption of protons during the reduction process should be studied as the process might occur differently at a microscale. The production of ammonia (NH_3) and nitric oxide (NO) from over-reduction might be measured in the reduced solution to see if this was part of the source of error.

Using zinc or photo-induced reduction of nitrate (NO_3^-) to nitrite (NO_2^-) (i.e. with a low pressure mercury lamp) would eliminate the environmental concerns associated with this method and its reliance on heavy metals as catalysts. Working with a UV transparent material would also largely increase the range of multistep reactions practical for inclusion onto a microfluidic disc.

Chapter 7

CONLUSIONS AND FUTURE DIRECTIONS

The objectives of this research, the development of a centrifugal microfluidic device for the detection of environmentally important chemical species including, nitrate, nitrite and hexavalent chromium by combining the fields of environmental science, centrifugal microfluidics and spectroscopy, have been met. More importantly, for the field of centrifugal microfluidics it has been shown that there are multiple strategies for the development of versatile general purpose instruments. These strategies can be implemented directly in the lab of the developer without significant expense or time. Several relevant key findings and future directions have been listed below. For greater detail see conclusions and future directions in the individual chapters.

Key Findings

- A spectrometer system capable of making fast, precise measurements was developed for use with centrifugal microfluidic discs.
- The detection of nitrite and hexavalent chromium by a single step reaction was demonstrated and included detection limits below the permissible drinking water limits, a large linear dynamic range and good precision.
- Implementation of hydrophilic capillary valves showed a high degree of reproducibility, and these valves are excellent candidates for controlling fluid movement on discs.

- A multi-step reaction for the detection of nitrate by reduction with cadmium to nitrite and derivatization was demonstrated. This proves that complex, multi step reactions are achievable on disc and opens the door to more sophisticated reaction chemistries. The modest analytical results of this particular reaction also highlight that further work is required to gain a better understanding of the precise processes that occur in centrifugal microfluidics.

Future Directions

- An in-depth study of the forces controlling capillary and hydrophobic valving on microfluidics discs is necessary. In particular, inclusion and characterization of combined filtration and valving would be a boon to centrifugal microfluidics of complex samples.
- Inclusion of a micro-reduction column on the disc, using cadmium or zinc to increase the precision and accuracy of the reduction of nitrate.
- Expansion of the basic design innovations (dry reagent pellets, capillary valves, efficient mixing and spectroscopic detection) presented in this thesis to include other single or multiple step reactions for the measurement of environmentally important species. There is a vast and untapped literature of "classic" wet chemical and colorimetric analyses that were largely abandoned with the advent of modern laboratory-based instrumental methodologies (e.g. chromatography, mass spectrometry, atomic spectroscopy) that are amenable to centrifugal microfluidic assays.

REFERENCES

1. Townsend, A.R., et al., *Human health effects of a changing global nitrogen cycle.* Frontiers in Ecology and the Environment, 2003. **1**(5): p. 240-246.
2. Boyer, E.W., et al., *Anthropogenic nitrogen sources and relationships to riverine nitrogen export in the northeastern USA.* Biogeochemistry, 2002. **57**(1): p. 137-169.
3. Galloway, J.N., et al., *Nitrogen cycles: past, present, and future.* Biogeochemistry, 2004. **70**(2): p. 153-226.
4. Sprent, J.I., *The Ecology of the Nitrogen Cycle.* 1987, Cambridge: Cambridge University Press. 151.
5. Van Breemen, N., et al., *Where did all the nitrogen go? Fate of nitrogen inputs to large watersheds in the northeastern USA.* Biogeochemistry, 2002. **57**(1): p. 267-293.
6. Moorcroft, M.J., J. Davis, and R.G. Compton, *Detection and determination of nitrate and nitrite: a review.* Talanta, 2001. **54**(5): p. 785-803.
7. Ghassemzadeh, F., et al., *The analysis of nitrate in highly saline waters.* International Journal of Salt Lake Research, 1997. **6**: p. 269-278.
8. Jungreis, E., *Estimation of Micro Quantities of Nitrate in Water with a Single Tablet-Formed Reagent.* Microchemical Journal, 1985. **32**(2): p. 143-147.
9. Oliveira, S.M., T. Lopes, and A. Rangel, *Spectrophotometric determination of nitrite and nitrate in cured meat by sequential injection analysis.* Journal of Food Science, 2004. **69**(9): p. C690-C695.
10. Sebranek, J.G. and J.B. Fox, *A Review of Nitrite and Chloride Chemistry - Interactions and Implications for Cured Meats.* Journal of the Science of Food and Agriculture, 1985. **36**(11): p. 1169-1182.
11. Verdon, C.P., B.A. Burton, and R.L. Prior, *Sample pretreatment with nitrate reductase and glucose-6-phosphate-dehydrogenase quantitatively reduces nitrate while avoiding interference by NADP(+) when the Griess reaction is used to assay for nitrite.* Analytical Biochemistry, 1995. **224**(2): p. 502-508.

12. Melchert, W.R., C.M.C. Infante, and F.R.P. Rocha, *Development and critical comparison of greener flow procedures for nitrite determination in natural waters.* Microchemical Journal, 2007. **85**(2): p. 209-213.

13. Al-Okab, R.A. and A.A. Syed, *Novel reactions for simple and sensitive spectrophotometric determination of nitrite.* Talanta, 2007. **72**(4): p. 1239-1247.

14. McAdam, E.J. and S.J. Judd, *Denitrification from drinking water using a membrane bioreactor: Chemical and biochemical feasibility.* Water Research, 2007. **41**(18): p. 4242-4250.

15. Kiso, Y., et al., *Visual determination of nitrite and nitrate in waters by color band formation method.* Chemosphere, 2006. **64**(11): p. 1949-1954.

16. Lu, C., et al., *Flow-injection chemiluminescent determination of nitrite in water based on the formation of peroxynitrite from the reaction of nitrite and hydrogen peroxide.* Analytica Chimica Acta, 2002. **474**(1-2): p. 107-114.

17. Griess, J.P., *"Griess' reagent".* Ber. Dtsch. Chem. Ges., 1879. **12**: p. 426-427.

18. Ivanov, V.M., *The 125th anniversary of the Griess reagent.* Journal of Analytical Chemistry, 2004. **59**(10): p. 1002-1005.

19. Marzinzig, M., et al., *Improved methods to measure end products of nitric oxide in biological fluids: Nitrite, nitrate, and S-nitrosothiols.* Nitric Oxide-Biology and Chemistry, 1997. **1**(2): p. 177-189.

20. Greenberg A E, E.A.D., Clesceri L S, Rice E W, ed. *Standard Methods for Examination of Water and Wastewater.* 21st ed. 2005, American Public Health Association, American Water Works Association, Water Environment Federation (Port City Press): Baltimore, MD. 1368.

21. Zunic, G., S. Spasic, and Z. Jelic-Ivanovic, *Simple and rapid method for the measurement of nitrite and nitrate in human plasma and cerebrospinal fluid by capillary electrophoresis.* Journal of Chromatography B, 1999. **727**(1-2): p. 73-79.

22. Wetters, J.H. and K.L. Uglum, *Direct spectrophotometric simultaneous determination of nitrite and nitrate in ultraviolet.* Analytical Chemistry, 1970. **42**(3): p. 335-&.

23. Sandford, R.C., A. Exenberger, and P.J. Worsfold, *Nitrogen cycling in natural waters using in situ, reagentless UV spectrophotometry with simultaneous determination of nitrate and nitrite.* Environmental Science & Technology, 2007. **41**(24): p. 8420-8425.

24. Zhang, J.Z. and C.J. Fischer, *A simplified resorcinol method for direct spectrophotometric determination of nitrate in seawater.* Marine Chemistry, 2006. **99**(1-4): p. 220-226.

25. Shiddiky, M.J.A., M.S. Won, and Y.B. Shim, *Simultaneous analysis of nitrate and nitrite in a microfluidic device with a Cu-complex-modified electrode.* Electrophoresis, 2006. **27**(22): p. 4545-4554.

26. Fanning, J.C., *The chemical reduction of nitrate in aqueous solution.* Coordination Chemistry Reviews, 2000. **199**: p. 159-179.

27. Motomizu, S. and M. Sanada, *Photoinduced reduction of nitrate to nitrite and its application to the sensitive determination of nitrate in natural-waters.* Analytica Chimica Acta, 1995. **308**(1-3): p. 406-412.

28. Kim, S.H., S.H. Song, and Y.J. Yoo, *Characteristics of mediated enzymatic nitrate reduction by gallocyanine-bound nanoporous electrode.* Journal of Microbiology and Biotechnology, 2006. **16**(4): p. 505-510.

29. Gonzalez, P.J., et al., *Bacterial nitrate reductases: Molecular and biological aspects of nitrate reduction.* Journal of Inorganic Biochemistry, 2006. **100**(5-6): p. 1015-1023.

30. Anderson, L., *Simultaneous spectrophotometric determination of nitrite and nitrate by flow injection analysis.* Analytica Chimica Acta, 1979. **110**(1): p. 123-128.

31. Jannasch, H.W., K.S. Johnson, and C.M. Sakamoto, *Submersible, osmotically pumped analyzers for continuous determination of nitrate in situ.* Analytical Chemistry, 1994. **66**(20): p. 3352-3361.

32. Stainton, M.P., *Simple Efficient Reduction Column for Use in Automated Determination of Nitrate in Water.* Analytical Chemistry, 1974. **46**(11): p. 1616-1616.

33. Gal, C., W. Frenzel, and J. Moller, *Re-examination of the cadmium reduction method and optimisation of conditions for the determination of nitrate by flow injection analysis.* Microchimica Acta, 2004. **146**(2): p. 155-164.

34. Jones, M.N., *Nitrate Reduction by Shaking with Cadmium - Alternative to Cadmium Columns.* Water Research, 1984. **18**(5): p. 643-646.

35. Nydahl, F., *Optimum conditions for reduction of nitrate to nitrite by cadmium* Talanta, 1976. **23**(5): p. 349-357.

36. Mir, S.A., *An improved zinc reduction method for direct determination of nitrate in presence of nitrite.* Asian Journal of Chemistry, 2007. **19**(7): p. 5703-5710.

37. Chow, T. and M.S. Johnstone, *Determination of nitrate in sea water.* Analytica Chimica Acta, 1962. **27**(C): p. 446-453.

38. Matsumoto, H. and S. Miyazima, *Colorimetric Determination of No-2-N and No-3-N in Water Samples by a Sulfanilamide Diazotation Method after Reduction with Zinc Powder.* Eisei Kagaku-Japanese Journal of Toxicology and Environmental Health, 1982. **28**(1): p. 1-7.

39. Bruus, H., *Theoretical Microfluidics.* Oxford Master Series in Physics Ser. 2007, New York City: Oxford University Press US. 364.

40. Haeberle, S. and R. Zengerle, *Microfluidic platforms for lab-on-a-chip applications.* Lab on a Chip, 2007. **7**(9): p. 1094-1110.

41. Nguyen, N.-T. and S.T. Wereley, *Fundamentals and Applications of Microfluidics.* Microelectromechanical Systems Ser. 2002, Boston: Artech House. 471.

42. Manz, A., N. Graber, and H.M. Widmer, *Miniaturized Total Chemical-Analysis Systems - a Novel Concept for Chemical Sensing.* Sensors and Actuators B-Chemical, 1990. **1**(1-6): p. 244-248.

43. Dittrich, P.S., K. Tachikawa, and A. Manz, *Micro total analysis systems. Latest advancements and trends.* Analytical Chemistry, 2006. **78**(12): p. 3887-3907.

44. West, J., et al., *Micro total analysis systems: Latest achievements.* Analytical Chemistry, 2008. **80**(12): p. 4403-4419.

45. Marle, L. and G.M. Greenway, *Microfluidic devices for environmental monitoring.* Trac-Trends in Analytical Chemistry, 2005. **24**(9): p. 795-802.

46. Gardeniers, H. and A. Van Den Berg, *Micro- and nanofluidic devices for environmental and biomedical applications.* International Journal of Environmental Analytical Chemistry, 2004. **84**(11): p. 809-819.

47. Majidi, V. and C. Hassell, *Miniaturized instrumentation for field applications: General considerations for environmental sensor networks.* International Journal of Environmental Analytical Chemistry, 2004. **84**(14-15): p. 1111-1121.

48. Ma, L., et al., *Simultaneous determination of nitrate and nitrite ion by micro-flow injection analysis.* Bunseki Kagaku, 1998. **47**(6): p. 375-380.

49. Petsul, P.H., G.M. Greenway, and S.J. Haswell, *The development of an on-chip micro-flow injection analysis of nitrate with a cadmium reductor.* Analytica Chimica Acta, 2001. **428**(2): p. 155-161.

50. Wu, C.H. and J. Ruzicka, *Micro sequential injection: environmental monitoring of nitrogen and phosphate in water using a "Lab-on-Valve" system furnished with a microcolumn.* Analyst, 2001. **126**(11): p. 1947-1952.

51. Motomizu, S., M. Oshima, and L. Ma, *On-site analysis for phosphorus and nitrogen in environmental water samples by flow-injection spectrophotometric method.* Analytical Sciences, 1997. **13**: p. 401-404.

52. Hirakawa, K., I. Yoshida, and D. Ishii, *Development of an analytical method using ultra-micro flow.* Bunseki Kagaku, 1998. **47**(6): p. 341-348.

53. Skogvold, S.M., et al., *Electrochemical properties of silver-copper alloy microelectrodes for use in voltammetric field apparatus.* Analytical and Bioanalytical Chemistry, 2006. **384**(7-8): p. 1567-1577.

54. Chen, Y.P., et al., *Simultaneous Determination of Nitrate and Dissolved Oxygen under Neutral Conditions Using a Novel Silver-Deposited Gold Microelectrode.* Environmental Science & Technology, 2008. **42**(22): p. 8465-8470.

55. Liu, S.Y., et al., *Innovative solid-state microelectrode for nitrite determination in a nitrifying granule.* Environmental Science & Technology, 2008. **42**(12): p. 4467-4471.

56. Greenway, G.M., S.J. Haswell, and P.H. Petsul, *Characterisation of a micro-total analytical system for the determination of nitrite with spectrophotometric detection.* Analytica Chimica Acta, 1999. **387**(1): p. 1-10.

57. Fujii, S.I., et al., *Fluorometric Determination of Sulfite and Nitrite in Aqueous Samples Using a Novel Detection Unit of a Microfluidic Device.* Analytical Sciences, 2004. **20**(1): p. 209-212.

58. Baeza, M.D.M., et al., *Microflow injection system based on a multicommutation technique for nitrite determination in wastewaters.* Analyst, 2006. **131**(10): p. 1109-1115.

59. Duffy, D.C., et al., *Microfabricated centrifugal microfluidic systems: Characterization and multiple enzymatic assays.* Analytical Chemistry, 1999. **71**(20): p. 4669-4678.

60. McNeely, M., et al. *Hydrophobic microfluidics.* in *Proceedings of SPIE - The International Society for Optical Engineering.* 1999. Santa Clara, CA, USA: Society of Photo-Optical Instrumentation Engineers.

61. Feng, Y.Y., et al., *Passive valves based on hydrophobic microfluidics.* Sensors and Actuators a-Physical, 2003. **108**(1-3): p. 138-143.

62. Chen, J.M., P.C. Huang, and M.G. Lin, *Analysis and experiment of capillary valves for microfluidics on a rotating disk.* Microfluidics and Nanofluidics, 2008. **4**(5): p. 427-437.

63. Ducrée, J., et al., *The centrifugal microfluidic Bio-Disk platform.* Journal of Micromechanics and Microengineering, 2007. **17**(7): p. S103-S115.

64. Grumann, M., et al., *Batch-mode mixing on centrifugal microfluidic platforms.* Lab on a Chip, 2005. **5**(5): p. 560-565.

65. Steigert, J., et al., *Integrated sample preparation, reaction, and detection on a high-frequency centrifugal microfluidic platform.* JALA - Journal of the Association for Laboratory Automation, 2005. **10**(5): p. 331-341.

66. Madou, M., et al., *Lab on a CD.* Annual Review of Biomedical Engineering, 2006. **8**: p. 601-628.

67. Brenner, T., et al., *Frequency-dependent transversal flow control in centrifugal microfluidics.* Lab on a Chip, 2005. **5**(2): p. 146-150.

68. Gomez, V. and M.P. Callao, *Chromium determination and speciation since 2000.* Trac-Trends in Analytical Chemistry, 2006. **25**(10): p. 1006-1015.

69. Rowland, G.P., *Photoelectric colorimetry - An optical study of permanganate ion and of the chromium-diphenyl carbazide system.* Industrial and Engineering Chemistry-Analytical Edition, 1939. **11**: p. 0442-0445.

70. Allen, T.L., *Microdetermination of chromium with 1,5-diphenylcarbohydrazide.* Analytical Chemistry, 1958. **30**(3): p. 447-450.

71. Madou, M., *Fundamentals of Microfabrication: The Science of Miniaturization.* 2nd ed. 2002, Boca Raton, FL: CRC Press.

72. Xia, Y.S. and G.M. Whitesides, *Soft lithography.* Annual Review of Materials Science, 1998. **28**(1): p. 153-184.

73. Duffy, D.C., et al., *Rapid prototyping of microfluidic systems in poly(dimethylsiloxane).* Analytical Chemistry, 1998. **70**(23): p. 4974-4984.

74. Bartholomeusz, D.A., R.W. Boutte, and J.D. Andrade, *Xurography: Rapid prototyping of microstructures using a cutting plotter.* Journal of Microelectromechanical Systems, 2005. **14**(6): p. 1364-1374.

75. Ingle, J. and S.R. Crouch, *Spectrochemical Analysis.* 1998, Upper Saddle River, NJ: Prentice Hall. 590.

76. Davis, C.E., Leffler, R., Anderson, J.B., *Effect of pH on absorbance of azo dye formed by reaction between nitrite and sulfanilamide/N-(1-naphthyl)ethylenediamine in residual nitrite methods for foods.* Journal of the Association of Official Analytical Chemists, 1985. **68**(3): p. 485-488.

77. Hach_Company, *Method 8507 Nitrite Diazotization Method LR*, in *Method 8507.* 2005.

78. Keusch, P., *Azo Dye Formation*, in *Demonstration Experiment on Video.* 2003, Fakultät Chemie & Pharmazie der Universität Regensburg. p. 1.

79. No_Author, *Nitrate Analysis Using HACH Reagents*, in *Chemistry Projects @ Moro Cojo Slough.* 2002, California State University, Monteray Bay.

80. Hach_Company, *Method 8023 Hexavalent Chromium 1,5-Diphenylcarbohydrazide* in *DR/4000 procedure 0 -0.700 mg/L.* 2005.

81. Albright, L.D.B., A. J., *Comparisons of luminaires: Efficacies and system design*, in *International Lighting in Controlled Environments Workshop* 1994: Wisconsin University. p. 281-297.

82. Health_Canada, *Chromium*, E.a.W. Health, Editor. 1986: Ottawa. p. 6.

83. Kramer, K.J.M., *Inorganic certified reference materials in 'water' what do we have, what do we need?* Analyst, 1998. **123**(5): p. 991-995.

84. Kim, N., et al., *Automated microfluidic compact disc (CD) cultivation system of Caenorhabditis elegans.* Sensors and Actuators B-Chemical, 2007. **122**(2): p. 511-518.

85. Cho, Y.K., et al., *One-step pathogen specific DNA extraction from whole blood on a centrifugal microfluidic device.* Lab on a Chip, 2007. **7**(5): p. 565-573.

86. Lutz, S., Lang, P., Faltin, B. Haeberle, F., vonStetten, F., Zengerle, R., Ducree, J. . *Towards a Comprehensive Centrifugal Process Integration by Rotationally Induced Lyophilisate Dissolutin and Cell Lysis.* in *Eleventh International Conference on Miniaturized Systems for Chemistry and Life Sciences*. 2007. Paris France.

87. Cho, H., et al., *How the capillary burst microvalve works.* Journal of Colloid and Interface Science, 2007. **306**(2): p. 379-385.

88. Ducree, J., et al., *The centrifugal microfluidic bio-disk platform.* Journal of Micromechanics and Microengineering, 2007. **17**(7): p. S103-S115.

89. Skłodowska, A., M. Woźniak, and R. Matlakowska, *The method of contact angle measurements and estimation of work of adhesion in bioleaching of metals.* Biological Procedures Online, 1999. **1**(3): p. 114-121.

90. Bandilla, D. and C.D. Skinner, *Protein separation by monolithic capillary electrochromatography.* Journal of Chromatography A, 2003. **1004**(1-2): p. 167-179.

91. Vlckova, M., A.R. Stettler, and M.A. Schwarz, *Microchip affinity capillary electrophoresis: Applications and recent advances.* Journal of Liquid Chromatography & Related Technologies, 2006. **29**(7-8): p. 1047-1076.

92. Hach_Company, *Method 8192 Nitrate Cadmium Reduction Method*, Nitrate_8192_PP_LR.fm, Editor.

93. Hach_Company, *Reproducibility of Nitraver6 and Nitraver5*, A. LaCroix-Fralish, Editor. 2008: Montreal. p. Spoke with Hach Representative to discuss reproducibility and mixing issues. Date may not be correct, but is an estimate.

APPENDIX A: Comparison of Spectrometers

Specification	BWTek BTC111E	OceanOptics USB4000
Operating temperature	15 - 30 °C	-10 + 50 °C
Detector	TE cooled 2048-element liner silicon CCD array	TCD 1304AP linear CCD array
CCE Elements	2040 at 14µm x 200 µm per element	3648 pixels at 8 µm x 200 µm per element
Effective Range	200nm-1050nm (configuration dependent)	200-1100nm (configuration dependent)
Cooling temperature	10-15 °C	Not cooled
Spectrograph f#	3.0	4.0
Spectrograph Optical Layout	Crossed Czerny-Turner	Asymmetric crossed Czerny-Turner
Spectrograph Optics	Aspherical Optics with sensitivity enhancement option	N/A
Grating	600-1800 line/mm (multiple blaze wavelengths)	600 - 2400 line/mm
Slit	10-800 µm x 1000 µm (configuration dependent)	5 - 200µm (configuration dependent)
Optical Resolution	0.3 -- > 10nm FWHM	0.3nm -10nm FWHM
Stray light	0.1% at 632 nm	<0.05% at 600 nm
Digitizer Resolution	16 bit (65,535 to 1)	16 bit (65,535 to 1)
Digitizer Speed (ADC)	500 kHz	3 MHz
External Trigger	Aux external port, built in software control	Aux external port, several modes
Integration time	9 - 65,535 ms w/multiplier (multiplier or 1, 2-16 s)	10 µs - >60 s spectroscopic (3.8ms - 10 s TIT)
Data Transfer Speed *readout rate	50 to <100 spectra per second	1 per 5ms = 12000 per second *1 MHz
Computer interface	USB1.1 or 2.0	USB 2.0 or 2 wire RSS-232
Operating Software	Windows ME, 2000, or XP	Windows 98/Me/2000/XP, Mac OS X and Linux with USB port; Any 32-bit Windows OS with serial port
Weight	600 g	190 g
Cost	3144 USD (quoted with filter) Free software	Starting at 2309 USD (from web) Software 199USD
Cooled	Yes	No
Shutter Mode	No (only external shutter)	Yes
Sensitivity	75 photons/count at 400 nm; 41 photons/count at 600 nm (estimated)	130photons/count at 400nm, 60 at 600nm
Power	5V DC @ <1.2A with ext supply	230 mA at +5VDC need ext supply if trigger with RS232
Filters	Linear variable filter	2nd and 3rd order rejection
Dark Noise	RMS dark is usually between 35-45 counts	24 counts at RMS for 32000 count saturation 50 for 65000
Signal-to-Noise	Peak S/N of 251 and an off-peak S/N of 1133	300:1 (at full signal)
Spectral resolution	<1.5nm	<1.5nm